Forest fire detection for near real-time monitoring using geostationary satellites

Tawanda Manyangadze
March, 2009

Course Title:	Geo-Information Science and Earth Observation for Environmental Modelling and Management
Level:	Master of Science (Msc)
Course Duration:	September 2007 - March 2009
Consortium partners:	University of Southampton (UK) Lund University (Sweden) University of Warsaw (Poland) International Institute for Geo-Information Science and Earth Observation (ITC) (The Netherlands)
GEM thesis number:	2007-07

Forest fire detection for near real-time monitoring using geostationary satellites

by

Tawanda Manyangadze

Thesis submitted to the International Institute for Geo-information Science and Earth Observation in partial fulfilment of the requirements for the degree of Master of Science in Geo-information Science and Earth Observation for Environmental Modelling and Management

Thesis Assessment Board

Chair: Dr. Ir. C.M.M. Mannaerts

External Examiner: Prof. Kasia Dabrowska-Zielinska

Internal Examiner: Ms. Ir. L.M. van Leeuwen

First Supervisor: Dr. B.H.P. Maathuis

Second Supervisor: Dr. Y.A. Hussin

ITC International Institute for Geo-Information Science and Earth Observation
Enschede, The Netherlands

Disclaimer

This document describes work undertaken as part of a programme of study at the International Institute for Geo-information Science and Earth Observation. All views and opinions expressed therein remain the sole responsibility of the author, and do not necessarily represent those of the institute.

Abstract

Forest fires are an important component of the savanna, tundra and boreal forest ecosystems. The increasing rate of the occurrence of fires however has increased the concern over their impacts on climate change and fragile ecosystems. This requires efficient and effective methods in forest fire detection for near real-time monitoring so as to minimize these impacts. Remote sensing has been widely used in active forest fire detection; however there are some limitations in contextual algorithms which are used in forest fire detection. These contextual algorithms are greatly affected by clouds and different land cover types such as land and water with inherent temperatures included in the N x N matrix and this brings errors. As a step towards minimizing these problems an automated multi-temporal threshold algorithm was developed in this study using MSG satellite and ground fire data from Portugal. The algorithm is based on temperature anomalies detected in IR3.9 channel and the difference between IR3.9 and IR10.8 channels as well as the solar zenith angles for day, night and twilight conditions. Thresholds were set to determine actual fires and possible fires depending on how far the temperature of a particular point or pixel deviates from the normal background temperature which is estimated using the images directly prior to the actual image. The accuracy of the algorithm was compared with that of the MSG FIR-G product. The McNemar's test was used for significance test of the difference between the multi-temporal threshold algorithm and the MSG FIR-G product which uses a contextual algorithm. This study shows that the multi-temporal threshold algorithm has higher fire detection rate (50%) as compared to MSG FIR-G (3.7%) when ground data from Portugal was used for validation. There is a significant difference between these methods (McNemar's test (x^2) = 5.45, df = 1, p-value = 0.0196). The superiority of the multi-temporal threshold algorithm over the contextual algorithm and significant difference between these methods was also confirmed in Southern Africa when MODIS fire product was used for validation. The automated procedure takes less than 15 minutes to produce the fire map, so it can cope with MSG satellite 15 minutes temporal resolution. Therefore the multi-temporal threshold algorithm performs better than the contextual algorithms in forest fire detection however there are some outstanding problems such as the transparent clouds that are not easily detected which may increase the errors in fire detection. Although this method was developed based on Portugal data it has been shown that it can be applied to other areas in the view of MSG satellite. This method can be easily adapted to other geostationary satellites and only the solar zenith angles have to be specific to the particular satellite.

Acknowledgements

I am very grateful to the European Union through the Erasmus Mundus scheme for awarding me a scholarship to undertake this course. It was a wonderful opportunity I had to study in four European countries. The course would not have been effective without the commitment of the consortium coordinators Prof. Andrew Skidmore of ITC, Prof. Terry Dawson of Southampton University, Prof. Petter Pilesjo of Lund University and Prof. Katarzyna Dabrowska of Warsaw University; together with the program secretaries. I greatly appreciate the dedication and professionalism of all my lecturers in the four universities.

My greatest gratitude goes to my supervisors Dr. B.H.P. Maathuis and Dr. Y.A. Hussin; for their invaluable ideas, opinions, suggestions, and guidance throughout all the phases of this research. My profound appreciation goes to Tânia Rodrigues Pereira (National Forest Authority-Portugal) for providing me with the data for fires in Portugal for 2007 which was not on the website on the time of this study. I would like to pass my gratitude to EUMETSAT staff especially Debbie Richards who provided me with some guiding material on processing of MSG data. I also give much thanks to the Working on Fire (WoF) staff in South Africa for their excellent communication during my studies and giving some information on fires in South Africa. I greatly appreciate Nuno Curado and Fernanda Henderikx Freitas' assistance in exploring and translating the Portuguese websites and all those I have not mentioned, who also contributed to the success of this piece of work.

I specially thank my GEM classmates for their friendship and moral support during the whole course. Above all, Vhusomuzi, Betty, Justice, Daphne, Rory, Tesfaye Suz and Kath; I felt your presence. I also thank Mhosisi Masocha (ITC PhD student) for support and encouragement during my research period. ITC SADC group, ITC Zimbabwean community and the ITC fellowship you made me feel home away from home.

My heartfelt thanks go to my parents for their love, encouragement and support; and to all my sisters. I therefore dedicate this research to my young sister Tatenda to her I am a source of inspiration. Above all, I give glory and thanks to my LORD, Jesus Christ, for His power and wisdom.

Table of contents

List of figures

List of tables

Acronyms

MSG – Meteosat Second Generation
SEVERI – Spinning Enhanced Visible and Infrared Imager
GOES - Geostationary Operational Environmental Satellites
MTSAT - Multi-functional Transport Satellite
JAMI – Japan Advanced Meteorological Imager
SR – Spatial Resolution
IFOV – Instantaneous Field of View
MVIRI – Meteosat Visible and InfraRed Imager
S-VISSR – Stretched Visible and Infrared Spin Scan Radiometer
MODIS – Moderate Resolution Imaging Spectroradiometer
EUMETSAT – European Organisation for the Exploitation of Meteorological Satellites
CGMS - Coordination Group for Meteorological Satellites
TOA – Top of Atmosphere
AVHRR - Advanced Very High Resolution Radiometer
NOAA - National Oceanic and Atmospheric Administration
METOP - Meteorological Operational
ABBA – Automated Biomass Burning Algorithm
MPEF – Meteorological Products Extraction Facility
FIR-G – MSG – Fires product, Gridded Format
AFMA – Active Fire Monitoring Algorithm
ALICE – Absolute Local Index of Change of the Environment
UTC – Coordinated Universal Time
ASTER - Advanced Spaceborne Thermal Emission and Reflection Radiometer
FIRMS – Fire Information for Resource Management system
AWiFS - Advanced Wide Field Sensor
AFIS – Advanced Fire Information Systems
SAFNET – Southern African Fire Network
DTM – Diurnal (Daily) Temperature Model
DCM – Diurnal (Daily) Cycle Model
GOFC-GOLD – Global Observation of Forest and Land Cover Dynamics
WoF – Working on Fire
ILWIS – Integrated Land and Water Information System

1. Introduction

1.1. Background

Fire is an important factor in the ecology of savanna, tundra and boreal forests ecosystems. Forest fires were once a natural phenomenon that played a very critical role in shaping species distribution and contributed to the persistence of fire dependent species, and helped the natural evolution of species. These days world fires are mainly caused by human pressure on the environment (San-Miguel-Ayanz et al., 2005). It was noted that about 5% of forest fires in Europe are of natural origin (San-Miguel-Ayanz et al., 2005) and fire is a fundamental part of land management in many parts of the world especially in the tropics (Kaufman et al., 1998).

The increase in the outbreak of fires has great negative impacts on the environment and socio-economic systems of many nations. Groot, (2007) noted that forest fires can have a wide range of negative impacts on human safety, health, regional economies, global climate change and fire sensitive ecosystems. It is estimated that around 2500 Mt of biomass are burnt every year over Africa, that is around half of the biomass which burn per year in the whole world (Arino and Melinotte, 1998). IPCC (1995) noted that the effect of biomass burning aerosols and aerosols from industrial activities has increased the uncertainty in assessing the anthropogenic climate change (Kaufman et al., 1998). This highlights the need to detect and control the fires as near real time as possible so as to reduce their impacts on the environment.

There are different methods used in detecting the forest fires. These include ground stations, airborne and remote sensing systems. The ground stations use the human surveillance and ground automatic detection systems that make use of cameras on towers and buildings and the airborne is also based on human surveillance from planes (San-Miguel-Ayanz et al., 2005). These two methods are limited by the costs and area covered by the detection and monitoring system. The detection of fires by satellites is significant from the operational and economical perspectives as this help to monitor very large areas. The satellite systems provide data at lower costs and they have higher data acquisition frequency which is critical for real-time fire monitoring.

Forest fire monitoring by remote sensing can be achieved through the use of polar-orbiting and geostationary satellites. The polar orbiting satellites that are used in fire detection and monitoring include MODIS, AVHRR, ASTER and Landsat. The application of these satellites is limited by their temporal resolutions. Their low temporal resolution makes them unable to detect active fires as near real-time as possible. This makes the geostationary satellites such as GOES and MSG more suitable for near-real time fire detection and monitoring as they give continuous data over the same position on earth in a short period of time. The International panel for Global Observation of Forest and Land Cover Dynamics (GOFC-GOLD) is working on many projects that are trying to link ground based and satellite data collection to help develop a global near real-time fire monitoring and early warning system. Groot et al., (2007) highlighted that the goal of GOFC-GOLD fire programme is going to be achieved by setting up an operational global geostationary fire monitoring network using current geostationary satellites such as GOES, MSG, MTSAT and FY-2C and future platforms like Indian INSAT-3D, Russian GOMS Electro L MSU-GS and Korean COMS. However this can only be fully achieved if there are algorithms that are developed and incorporated into these systems to detect the forest fires in a near real-time. This study proposes a multi-temporal approach that can be used to detect forest fires using geostationary satellites.

1.2. Research problem

Fire causes irreversible damage to fragile natural ecosystems and greatly affects the socio-economic systems of many nations especially in the tropics where forest fires are more prevalent. Early detection of these fires may help reduce these impacts. Currently, there are efforts to develop satellite systems that can detect active fires for early warning systems (Groot et al., 2007). These efforts include the use of polar-orbiting satellites such as MODIS, AVHRR, ASTER and Landsat as well as geostationary satellites such as MSG and GOES. The application of polar-orbiting satellites on near-real time active fire detection is limited by their low temporal resolutions that lead to inevitable lag in the dissemination of data. This has limited the use of these systems for operational near real-time forest fire detection (San-Miguel-Ayanz et al., 2005). The polar orbiting satellites may not detect small fires and those of short duration. This gives the need and motivation to develop the additional and/or alternative algorithms that are applicable to near-real time active fire detection using the geostationary satellites such as MSG and GOES.

The geostationary satellites are positioned at a fixed height (about 36 000km) above the earth and they are capable of giving continuous data on the state of environment on the same position. This is important for near-real time active fire detection and monitoring. MSG SEVERI is one of the geostationary satellites that are used to detect and monitor active fires as it images the earth every 15 minutes. A few algorithms (contextual and threshold) were developed for near real time active fire detection using MSG SEVERI satellite. Calle et al., (2004) developed the contextual algorithm (for MSG) using 3.9µm and 10.8µm using the N x N spatial matrix of pixels to calculate the mean and standard deviation which were used in the thresholds to detect fire. Hassini et al., (2009), developed the threshold algorithm using 3.9µm and 10.8µm as well. MSG satellite currently uses this method for active fire detection and monitoring (EUMETSAT and CGMS, 1999)

These operational contextual and threshold methods for active fire detection utilize information from one image and have been reported as giving a number of false alarms (Kaufman et al., 1998, San-Miguel-Ayanz et al., 2005). The use of one image may be greatly affected by cloud cover and different land covers with different temperatures which may give false fire alarms. These algorithms tends to miss some of the fires due to the low fire intensity especially during the night (San-Miguel-Ayanz et al., 2005). However given these limitations of contextual and threshold algorithms, little progress has been reported about using temporal dimension of satellite data (Koltunov and Ustin, 2007). There is need for multi-temporal threshold algorithms that can be used by geostationary satellites such as MSG and GOES to detect the active fires. The multi-temporal approach may have a great potential for near real time active fire detection as it considers the temperature of a point over a period of time. The automated multi-temporal active fire detection algorithms may help to establish an effective and efficient early warning system to monitor and assess the negative social, economic and environmental effects of forest fires.

1.3. Research Objectives

1.3.1. General objective

The main objective of this study is to develop an automated system for near real-time fire detection and monitoring using geostationary satellites.

1.3.2. Specific objectives and research questions

The table below shows the specific objectives and research questions of this study.

Table 1.1 Specific objectives and research questions

Specific objectives	**Research questions**
1. To develop an algorithm to detect the temperature anomalies for fire detection using 3.9 and 10.8µm MSG SEVERI satellite channels using a multi-temporal threshold method.	1. What capabilities does MSG SEVIRI have to detect temperature anomalies using multi-temporal method? 2. Is the difference between 3.9µm and 10.8 µm channels important for fire detection in multi-temporal algorithm? 3. How can these temperature anomalies be used to detect fires?
2 To validate the algorithm using actual fire data from Portugal and South Africa and compare the accuracy with MPEF (FIR-G) fire product from MSG satellite.	4. How does the accuracy of the algorithm developed in this study and the MPEF fire product differ when actual fire data and MODIS fire product are used for validation? 5. Is there a need for the algorithm to be improved to detect small and short duration fires by changing the thresholds and correction of CO_2 absorption on IR3.9 channel?
3 To develop a near real time automated procedure to determine the optimum multi-temporal threshold for the algorithm for fire detection using MSG SEVIRI geostationary satellite.	6. How can the procedure for the multi-temporal threshold algorithm be automated to cope with the temporal resolution of MSG (15 minutes)?

1.4. Hypotheses

This study set out to test the hypotheses outlined below.

1. H_o: Multi-temporal threshold and contextual-threshold algorithms have equal performance on forest fire detection.

   H_1: Multi-temporal threshold and contextual-threshold algorithms do not have equal performance on forest fire detection.

2. H_o: Multi-temporal threshold algorithm with CO_2 correction has equal performance with the multi-temporal threshold without CO_2 correction.

   H_1: Multi-temporal threshold algorithm with CO_2 correction does not have equal performance with the multi-temporal threshold algorithm without CO_2 correction

2. Literature Review

This chapter discusses some of the critical issues in forest fire detection using remote sensing. These include why geostationary satellites may be considered most suitable for forest fire detection and monitoring, overview of the spectral channels used in forest fire detection and a detailed analysis of the algorithms that are widely used in global forest fire detection projects and validation of satellite fire products.

2.1. Why geostationary satellites?

Geostationary satellites are always on the fixed position above the earth (approximately 36000km) and they provide continuous data for the same place. This gives them an advantage over the polar orbiting satellites in their application in near-real time active forest fire detection and monitoring. Sensors on polar orbiting satellites have been widely used in active forest fire detection. These include AVHRR and MODIS and their general characteristics are shown in the table below.

Table 2.1 Polar orbiting satellites widely used in forest fire detection

Sensor	**Satellite**	**Spatial Resolution**	**Temporal Resolution**	**Swath Width**	**Channels and bands for fire detection**
AVHRR	NOAA	1.1 km	2 times in 24 hrs	2400 km	3a(1.6µm(Night)) 3b(3.9µm(Day)) 4 (11µm)
MODIS	Aqua/Terra	1 km at nadir	4 times in 24 hrs (2-day and 2-night)	2330 km	21 and 22 (3.9µm) 31 (10.8µm)

The temporal resolutions for polar orbiting satellites greatly discredit them from providing near real-time fire detection and monitoring system as compared to the geostationary satellites. Their spatial resolution is higher than that of the geostationary satellites which is critical for forest fire detection; however forest fires are a rapidly changing phenomenon which requires the application of satellites with high temporal resolution as well. The launch of the MSG SEVERI in 2002, the activation of GOES -9 in 2003 and the MTSAT-1R (Japanese Advanced

Meteorological Imager (JAMI) in 2005 has increased the possibilities of generating global fire products of high temporal resolution using geostationary satellites (Prins et al., 2004, Calle et al., 2008). Figure 2.1 below shows global coverage achieved by some of the geostationary satellites which are used in forest fire detection.

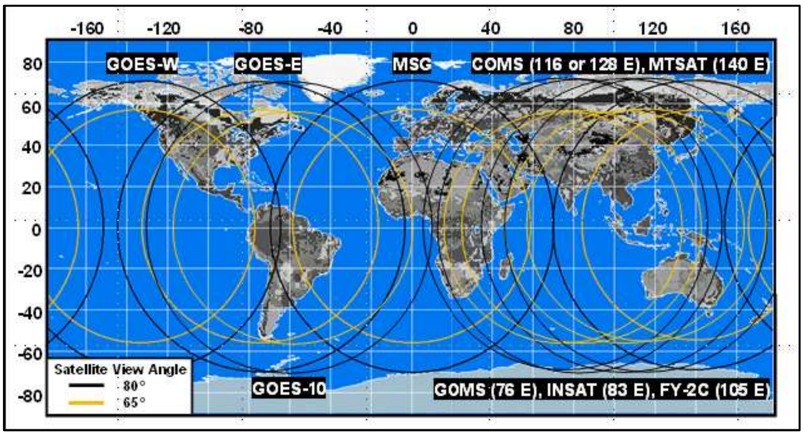

Figure 2.1 Components of a global geostationary fire monitoring system (Prins et al., 2007)

The GOFC-GOLD international panel is working towards the development and implementation of a global geostationary fire monitoring system using the geostationary satellites as highlighted in the diagram above (Prins et al., 2004, Groot et al., 2007). Fire detection is a necessity which will only be solved if the geostationary satellites prove their capacity in detecting small fires and show their applicability in providing the early warnings of the occurrence of fires (Calle et al., 2004). This could be difficult to achieve as it is difficult to develop high spatial resolution thermal sensors (Calle et al., 2004), however, methods (algorithms) can be improved or developed so as to improve the performance of geostationary sensors in active forest fire detection.

2.2. Overview of Global Geostationary Satellites

The global geostationary satellites have different characteristics (Table 2.2) that are desirable for active forest fire detection. These sensors have different capabilities in detecting and monitoring forest fires hence the need to standardize them to create consistent fire products around the globe (Prins et al., 2004). This can be achieved by developing the methods or algorithms that are applicable to all sensors as well as different climatic regions and illumination conditions.

Table 2.2 Overview of Global Geostationary Fire Monitoring Capabilities (Prins et al. 2004)

Satellite & Sensor	Position	Active Fire Spectral Bands	IFOV (km)	SR (km)	Full Disk Coverage	3.9 µm Saturation Temperat-ure (K)	Minimum Fire Size at Equator (at 750 K) (ha)
MSG 8 (SEVIRI)	9.5^0 E	1 HRV 2 visible 1.6, 3.9 and 10.8 µm	1.6 4.8 4.8	1.0 3.0 3.0	15 minutes	~335 K	0.22
MSG 9 (SEVIRI)	0^0 E	1 HRV 2 visible 1.6, 3.9 and 10.8 µm	1.6 4.8 4.8	1.0 3.0 3.0	15 minutes	~335 K	0.22
GOES-11 (Imager)	135^0 W	1 visible 3.9 and 10.7 µm	1.0 4.0 (8.0)	0.57 2.3	3 hours	~322 K	0.15
GOES-12 (Imager)	75^0 E	1 visible 3.9 and 10.7 µm	1.0 4.0 (8.0)	0.57 2.3	3 hours	~335 K	0.15
MTSAT-1R (JAMI)	140^0 E	1 visible 3.7 and 10.8 µm	0.5 2.0		< 24 minutes	~320 K	0.03

In addition to the satellites in the table above, there are other two geostationary satellites; MET 7 (MVIRI) and FY 2C (S-VISSR) positioned at 57.5^0 E and 105^0 E which are also applied in forest fire detection. With temperature of 750^0 K as mentioned by Prins et al., (2004) in the table above the whole pixel may be detected as fire even if only a small fraction of pixel is covered by fire. However, it should be noted that the sizes of fires mentioned above may be difficult to detect considering the spatial resolution of the geostationary satellites.

2.3. Detailed characteristics of MSG satellite

Meteosat Second Generation (MSG) is a spin-stabilized satellite with a repeat cycle of 15 minutes which gives unprecedented multispectral observations of rapidly changing environment (Schmetz et al., 2002). It has a geostationary orbit at an altitude of 35 600km above the earth’s surface. MSG-8 has a rapid scan service

(RSS) which gives images in every five minutes which shows the advances in technology toward near-real time monitoring of rapidly changing environmental phenomenon such as forest fires. The rapid scan service (RSS) is only over the Northern part of the disk covering only one third of the full disk. The most important instrument on MSG is the Spinning Enhanced Visible and Infrared Imager (SEVERI) with 12 channels as shown in the table 2.3 below. SEVIRI instrument has spatial resolution of 3km and instantaneous field of view (IFOV) of 4.8km at nadir for channels 1-11 and these give full disk images. Channel 12 (High Resolution Visible (HRV)) has spatial resolution of 1km and IFOV of 1.67 and it covers half of the full disk in East to West direction (Schmetz et al., 2002). The images for channels 1-11 have 3712 x 3712 pixels and for channel 12 they have 11 136 x 11 136 pixels.

Table 2.3 Spectral characteristics of MSG satellite (Schmetz et al. 2002)

Channel no.		**Characteristics of spectral band (μm)**			**Main gaseous absorber or window**
		λcen	λmin	λmax	
1	VIS0.6	0.635	0.56	0.71	Window
2	VIS0.8	0.81	0.74	0.88	Window
3	NIR1.6	1.64	1.50	1.78	Window
4	IR3.9	3.90	3.48	4.36	Window
5	WV6.2	6.25	5.35	7.15	Water vapor
6	WV7.3	7.35	6.85	7.85	Water vapor
7	IR8.7	8.70	8.30	9.10	Window
8	IR9.7	9.66	9.38	9.94	Ozone
9	IR10.8	10.80	9.80	11.80	Window
10	IR12.0	12.00	11.00	13.00	Window
11	IR13.4	13.40	12.40	14.40	Carbon dioxide
12	HRV	Broadband (about 0.4 – 1.1)			Window/water vapor

2.4. An overview of the spectral channels for active forest fire detection

Fires have strong signal in the mid-infrared part of the electromagnetic spectrum which makes it the most suitable part of the spectrum for active fire detection (San-Miguel-Ayanz et al., 2005). There are two main channels (3.9 and 10.8) that are widely used for active forest fire detection. **T**he peak of the emission of radiance for blackbody surfaces is around 4µm (Wien’s Displacement Law) (Figure 2.2) and this corresponds with MSG channel IR3.9µm and the ambient temperature of 290K, the peak of radiance is approximately at 11µm (Figure 2.3) (MSG channel IR10.8)(EUMETSAT, 2007). Therefore IR3.9 channel is more sensitive to changes in temperatures than other channels and picks up hotspots caused by fires; hence it is mostly used in forest fire detection.

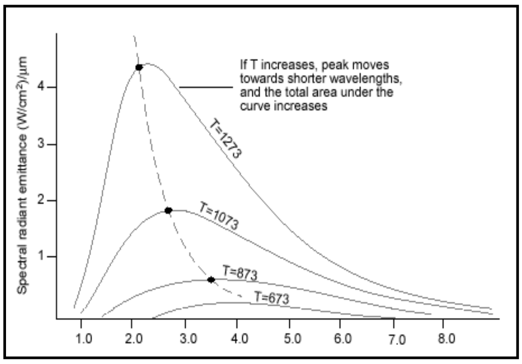

Figure 2.2 Black body Blackbody radiation curves based on Stefan-Boltzmann's law (Janssen and Huumeman, 2001)

In support of this (San-Miguel-Ayanz et al., 2005) noted that the mid-infrared spectral window is suitable for fire detection because it is far from the peak of the Earth and solar radiations at 9.7 and 0.5µm respectively. However the IR3.9 channel records the reflected energy from the sun and Earth's radiant energy during the day (Figure 2.3) and during the night it records the emitted energy from the earth only. This means that this channel has different responses during the day and night and during the day the channel can be saturated as temperatures go up. Saturation brightness temperature is regarded as the maximum temperature that can be derived from the sensor. This has been regarded by Prins et al., (2004). and (San-Miguel-Ayanz et al., 2005) as one of the limiting factors in the application of the 3.9 channel in forest fire detection and characterization (estimates of fire size and temperature). This greatly affects the temperature anomaly detection as all the signals that exceed the saturation limit may be given the saturation temperature (Li et al., 2000). The saturation point for MSG SEVERI (335K) is higher than most of the satellites and this may not pose a big problem in forest fire detection.

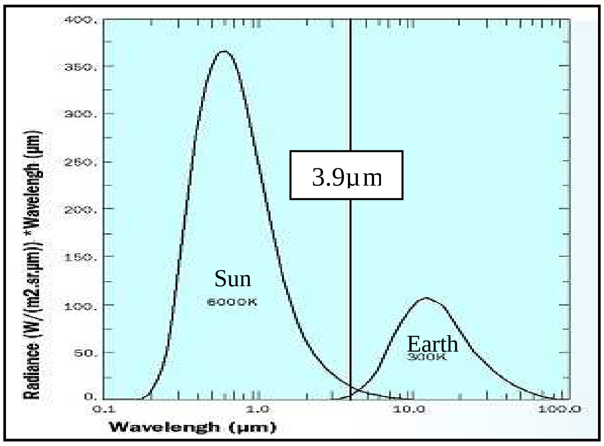

Figure 2.3 The effect of solar radiation on 3.9µm channel (EUMETSAT and CGMS, 1999)

Given this situation it shows that during the day the satellite measured temperature will not be true representative of the insitu temperatures (Figure 2.4) therefore the applications and algorithms should be different for day and night (Kerkmann, 2004).

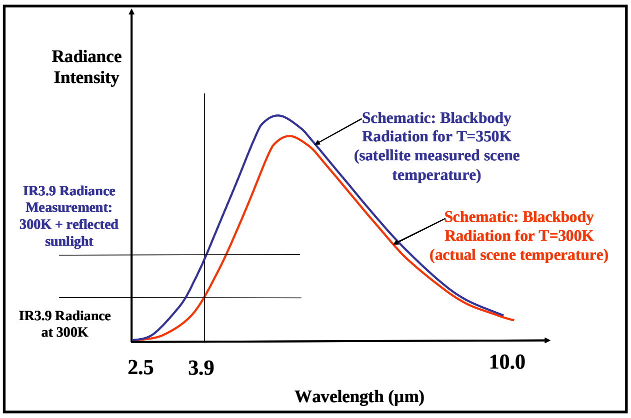

Figure 2.4 The effect of the solar radiation on 3.9 channel (Kerkmann 2004)

The 10.8 channel is not very sensitive to changes in temperature as compared to 3.9 channel hence the difference between the 3.9 and 10.8 is higher for fire pixels than for non-fire pixels (Hassini et al., 2009, Giglio et al., 2003). The IR3.9 channel has a stronger thermal response as compared to IR10.8 channel even if fire covers a small portion of the pixel (Philip, 2007) (Figure 2.5). Small, but very hot, sub-pixel regions can dominate the average pixel brightness temperature in IR3.9 channel (EUMETSAT and CGMS, 1999). This is important as it supports why IR3.9 and IR10.8 channels are used in forest fire detection.

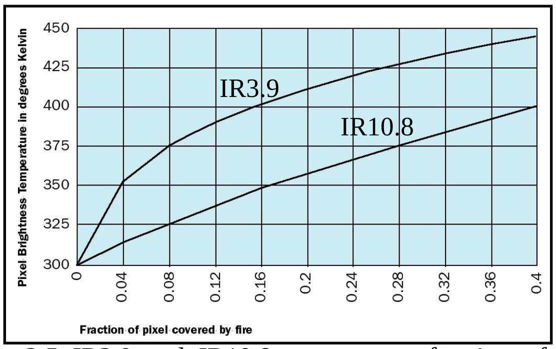

Figure 2.5 IR3.9 and IR10.8 response to fraction of pixel covered by fire (EUMATSAT and CGMS 1999; Philip 2007)

From figure 2.5 above it can be noted that the temperature in IR3.9 channel is always higher than in IR10.8 channel when there is fire. When the fire occupies 4% of the pixel the temperature in band IR3.9 gets up to 350^0 K and the temperature in IR10.8 channel is approximately 35^0 K lower than IR3.9 temperature.

The use of the TOA temperatures for forest fire detection may be affected by absorption in the atmosphere. Absorption of radiation generally occurs when the atmosphere prevents the transmission of radiation or energy to pass through the atmosphere (Campbell, 2006). The main absorbers include ozone (O_3), carbon dioxide (CO_2) and water vapour (H_2O) (Figure 2.6). There are two most important atmospheric windows: (i) 3.5 – 4.1µm and (ii) 10.5 – 12.5µm (Campbell, 2006). The first window corresponds with the MSG 3.9 channel and the second window corresponds with 10.8 MSG channel. The 10.5 – 12.5µm window is important for it approximately corresponds with the peak emission from the earth's surface. Although the 3.9 channel is regarded as atmospheric window channel it is close to the CO_2 absorption band at 4-5 microns (Kerkmann, 2004) so it is also affected by the CO_2 absorption (Figure 2.6). This may need to be corrected to improve the performance of the algorithms in forest fire detection.

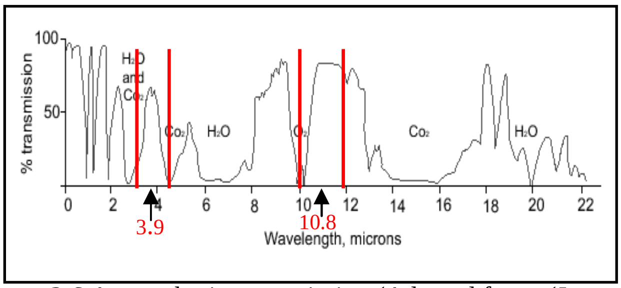

Figure 2.6 Atmospheric transmission (Adapted from (Janssen and Huurneman, 2001)

As shown in table 2.3, Channel 4 (IR3.9) stretches from 3.48 to 4.36 and channel 10 also extends from 9.8 to 11.8 µm and the effects of CO_2 absorption is shown in figure 2.6.

2.5. Effects of clouds on forest fire detection

Clouds greatly affect the TOA temperatures as they may lower the temperatures as measured by the satellites. Usually clouds have cold tops and hence low brightness temperatures and therefore fires under these clouds are missed as they can not be detected using temperatures at the top of atmosphere. There are some clouds such as cirrus which are thin and transparent and difficult to detect (Li et al., 2000, Giglio et al., 1999). This has been noted as a problem mainly in contextual algorithms as these clouds may not be detected and they finally affect the results as low temperature values induced by presence of clouds are used in the analysis. The contextual algorithms normally consider the use of 3x3 matrix in estimating the background temperature (section 2.6 below) therefore if there are some undetected clouds in this matrix it is most likely that the final result is biased. However this could also be a problem in multi-temporal algorithms and the accuracy of the results of any fire detection algorithm may be based on the accuracy of the cloud masking method applied.

2.6. Review of Operational fire detection algorithms

Currently most of the algorithms that are applied in forest fire detection are fixed threshold or contextual tests or both (Koltunov and Ustin, 2007). Most of these algorithms have been developed for the sensors such as MODIS and AVHRR on board of TERRA/AQUA and NOAA/METOP polar orbiting satellites respectively. The contextual algorithms were developed and are operational for AVHRR and MODIS (Kaufman et al., 1998, Giglio et al., 2003, Flasse and Ceccato, 1996, Justice et al., 2002). Threshold algorithms have been operational on AVHRR (Arino and Melinotte, 1998, Li et al., 2000).

2.6.1. Operational fire detection algorithms using geostationary satellites

A few algorithms have been developed so far for the active forest fire detection using geostationary satellites such as GOES, MTSAT-1R and MSG. Although these algorithms may be different from sensor to sensor depending on specifications it can be noted that the basic principles are similar to those that are in use for other instruments such as GOES, AVHRR and MODIS (Hassini et al., 2009). The algorithms that have been developed for active fire detection using geostationary satellites are discussed below.

2.6.2. Contextual algorithms

Contextual algorithms consider the background intensity as they attempt to predict the temperature of a pixel by calculating the average intensity by considering the neighbouring pixels (Koltunov and Ustin, 2007). Tests are used to decide whether it's a hot anomaly or not. A hot spot is considered a fire only if its temperature is above the temperature of its surrounding pixels (San-Miguel-Ayanz et al., 2005). Calle et al., (2004) developed the contextual algorithm for MSG using 3.9µm and 10.8µm using the N x N spatial matrix of pixels to calculate the mean and standard deviation which were used in the thresholds to detect fire. For a pixel to be classified as fire, it should meet the requirements of the threshold below.

$$T_{3.9\mu m} > \mu_{3.9\mu m} + f.\sigma_{3.9\mu m}$$
$$T_{3.9\mu m} - T_{10.8\mu m} > \mu_{dif} + f.\sigma_{dif}$$

Where, T is temperature for a pixel at 3.9µm, σ is standard deviation, µ is the mean of the selected N x N pixel and *f* is a critical value that determines the thresholds.

2.6.2.1. Threshold algorithms

These are basically fixed-threshold thermal tests (Koltunov and Ustin, 2007). In this case a pixel is considered as fire if its brightness temperature in one or more spectral bands exceeds a pre-specified fixed threshold. The algorithms are pixel based and they do not consider temperature in the neighbouring pixels to estimate the background temperature. Only a few if any fixed threshold algorithms were developed and are operational for the geostationary satellites. The most popular fixed thresholds were developed by Arino and Melinotte, (1998) and Li et al., (2000) for NOAA-AVHRRR (polar-orbiting satellite). Most of the algorithms developed for geostationary satellites are thresholding contextual algorithms discussed in section 2.6.2.2 below.

2.6.2.2. Thresholding Contextual algorithms

These algorithms include both contextual and fixed algorithms. The most popular algorithm of this kind is the GOES ABBA. This is a contextual multi-spectral thresholding algorithm that utilizes local dynamic threshold using GOES satellite imagery (San-Miguel-Ayanz et al., 2005) and it was made operational in 2002 (Prins et al., 2004). The algorithm requires that the brightness temperature detected at IR3.9 channel should be at least 4K greater than the average background brightness temperature. This threshold, however, can be reduced to 2K homogeneous regions allowing for the detection of smaller fires (Prins et al., 2004).

Hassini et al., (2009) developed a threshold algorithm (Active Fire Monitoring Algorithm) for MSG using the top of atmosphere temperatures in IR3.9 and IR10.8 channels. The thresholds are as shown in table 2.4 and figure 2.7 below.

Table 2.4 Thresholds for fire tests (Hassini et al., 2009)

	Threshold		**Active fires**	
Test	**Day**	**Night**	**Day ^{0}K**	**Night ^{0}K**
T4	Threshold 1	Threshold 5	315	290
SDev Ch4	Threshold 2	Threshold 6	4	4
SDev Ch9	Threshold 3	Threshold 7	2	2
T4- T9	Threshold 4	Threshold 8	10	5

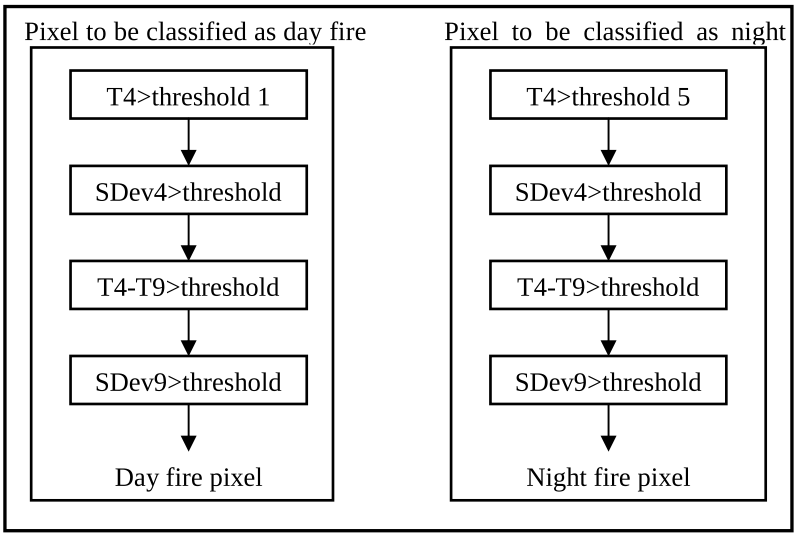

Figure 2.7 Active Fire Monitoring Algorithm **(**AFMA) (Hassini et al.,

The MSG satellite currently uses this method for active fire detection and monitoring (EUMETSAT, 2007) to produce the fire product (MPEF FIR-G). The difference is only on the threshold levels as shown in table 2.5 below:

Table 2.5 Thresholds for the four fire tests (EUMETSAT, 2007)

	Potential fire		**Fire**	
Test	**Day**	**Night**	**Day**	**Night**
IR3.9	310 K	290K	310K	290 K
StdDev 3.9	2.5 K	2.5 K	4 K	4 K
StdDev 10.8	2 K	2 K	2 K	2 K
IR3.9-IR10.8	8 K	0 K	10 K	5 K

In these thresholds the standard deviation for IR3.9 and IR10.8 is calculated using a 3x3 pixel around the hot spot. The day and night are defined with the local solar zenith angle. The solar zenith angle lower than 70^0 is considered as day and for night the solar zenith angle is higher than 90^0 and for the solar zenith angles between 70 and 90 the thresholds are linearly interpolated (EUMETSAT, 2007, Hassini et al., 2009) for example from 310 to 290^0 K for day to night respectively.

2.6.3. Limitations of the contextual and thresholding-contextual algorithms

Although there were some improvements on Kaufman et al., (1998) MODIS fire detection algorithm by Justice et al., (2002) some false fire detections were persistently observed in some deserts and sparsely vegetated land surfaces and in some cases small fires were not detected at all and most of these were mainly caused by the algorithms thresholds tests (Giglio et al., 2003). Giglio et al., (2003) noted that even the version 4 of MODIS fire detection algorithm has a few blatant false alarms and its performance is yet to be assessed in different conditions. Hawbaker et al., (2008) evaluated the accuracy of the MODIS active fire products in the United States and they obtained 82% fire detection rate when they used both Aqua and Terra combined. The detection rate was higher when the products from both MODIS sensors were combined but when considered individually Aqua had 73% and Terra obtained 66% (Hawbaker et al., 2008). The difference is mainly attributed to different overpasses of the two sensors. These results show that more can be done to improve the methods to increase the fire detection rates for near-real time monitoring.

Hassini et al., (2009) and EUMETSAT (2007) highlighted some of the problems that are clearly outstanding on their thresholding contextual algorithm (Active Fire Monitoring Algorithm) for MSG. These problems include: Undetected clouds, sub-pixel clouds, fire under thin Cirrus, mixed land and water scenes, inhomogeneous land surfaces, unknown land surface emissivity in IR3.9 channel and dusk and dawn with rapidly changing 3.9 channel values. This is mainly because pixel intensities of different objects are different and these may bring in errors when using the 3x3 kernel in contextual algorithms.

Algorithms that use fixed environmental temperature threshold can be effective when calibrated to the standard local conditions (San-Miguel-Ayanz et al., 2005) so cannot be applicable to global scale (Giglio et al., 1999). These methods can also miss some small fires of low intensity and can produce false fire alarms in overheated areas especially during summer. Ravail and San-Miguel-Ayanzi, (2002) in San-Miguel-Ayanzi, (2005) evaluated the performance of Falasse and Ceccato's, (1996) contextual algorithm in Spain in 1997 and 1998 on AVHRR and concluded that about 90% of the detected fires were false fires due to the overheating and by systematic error on land and water interfaces.

Calle et al., (2004) appreciate that in general the contextual procedure is reliable and a large number of errors is mainly attributed to the final statistical parameters. Although this may not be a general consensus amongst the researchers, to some extent its very difficult to set statistical parameters such as mean and standard deviation to the exact levels that they detect the fires totally free of false fire alarms and also without missing very small fires. In contextual algorithms water and clouds greatly affect the detection of the algorithms as water and cloud pixels are masked out and hence they are not included in the calculation of the mean and standard deviation of the temperatures that is used in the algorithms. The calculation of mean and standard deviation is abandoned if there are less than 3 pixels available for the calculation (Hassini et al., 2009) which means that some fires are missed in such circumstances.

2.6.4. Multi-temporal approach

With the limitations of the operational threshold and contextual algorithms mentioned above, Koltunov and Ustin, (2007) advocate for the development of additional and/or alternative methods that may have better performance as compared to the current ones. Koltunov and Ustin, (2007) noted the multitemporal approach may have a great potential in reducing the problems highlighted above because they will use a number of images unlike the operational algorithms that only use one image and yet little or no progress if any have been reported about using multi-temporal remote sensing data for fire detection. They also acknowledged that the method they proposed (non linear Dynamic Detection Model (DDM)) did not perform very well in forest fire detection. This shows that more attention or attempts should be given to multi-temporal algorithms for fire detection so as to yield better results.

Mazzeo et al., (2007) developed a multi-temporal robust satellite technique (RST) for forest fire detection. They developed an index (ALICE (Absolute Local Index of Change of the Environment).

$$\otimes_{MIR}(x,y,t) = \frac{[T_{MIR}(x,y,t) - \mu_{MIR}(x,y)]}{\sigma_{MIR}(x,y)}$$

Where (x,y,t) is the brightness temperature of the signal measured in the MIR channel at (x,y) location and time t; and $\mu_{MIR}(x,y)$ is the temporal mean and $\sigma_{MIR}(x,y)$ is the standard deviation.

This method considers the physical properties of the target and observational and environmental factors such as land cover, hour of pass, and viewing angle as conditions which determine the thermal signal measured by the satellite. This means that any changing event is regarded as anomalous if it produces a significant deviation from the natural normal behaviour of the signal measured under normal undisturbed conditions (Mazzeo et al., 2007). The authors pointed out that the method performed very well as it did not miss any fires during the validation phase, however they did not highlight which MIR bands or channels they used and they did not give the exact thresholds (to define fire (small or big) for the index as they used different values. This means that more research is required to develop more temporal algorithms for forest fire detection. This method however proved that temporal algorithms can perform better than contextual and threshold algorithms as it can be applied in any observational conditions: day or night and summer or winter.

Van den Bergh and Frost, (2005) proposed a multi-temporal approach for fire detection using MSG satellite data. This approach uses the Diurnal Cycle Model (DCM) and the kalman filter is used to filter the observed data and estimate the distribution of the difference between observed and predicted values and flag out statistically significant differences as possible fires. The DCM or Diurnal (Daily) Temperature Model (DTM) is a method that provides temperature variation for full day for given pixel and in this case the diurnal cycle is modelled using temperatures in IR3.9 channel (Udahemuka et al., 2008). On the validation of this method it missed 5 MODIS fire pixels and there is need for validation on a large data set (van den Bergh and Frost, 2005). The author claim that the algorithm performed better than the contextual and threshold algorithms on MSG although it cannot perform at the same level with the MODIS fire product at the present moment. However, (Udahemuka et al., 2008) highlighted the limitations of using the DCM in fire detection as some of the anomalies maybe due to partial or full cloud cover over a pixel, solar reflection, precipitation and land cover and wind fluctuations. This clearly shows that there is need for more research into other methods for active forest fire detection especially those that take advantage of the temporal domain of geostationary satellites such as MSG, GOES and MTSAT-1R.

2.6.5. Validation of fire products

Validation refers to the process of assessing satellite product quality or accuracy with independent reference data (Roy et al., 2005). Accuracy refers to the correctness of remotely sensed data as it measures the agreement between a standard assumed to be correct and classified image of unknown quality (Foody, 2001, Campbell, 2006). Although accuracy is a difficult property to measure and express (Shan-long et al., 2006), it is one of the strongest basis of scientific research as (Strahler et al., 2006) noted that maps or satellite products without associated accuracy data remain untested hypothesis.

Validation of active forest fire products is considered a difficult task which lacks well established procedures. There are different methods that have been applied in the validation of forest fire products. These include: (i) use of other remote sensed data for example ASTER on MODIS fire product (Csiszar et al., 2006). MODIS and AWiFS on MSG SEVERI (Calle et al., 2008), (ii) use of smoke plumes for assessment for example on AVHRR (Christopher et al., 1998) and smoke plumes SPOT for MODIS (Liew et al., 2003) (iii) fire locations compared with fire perimeters (Li et al., 2000). Ground based data is always the best for the validation of the remotely sensed data. Csiszar et al., (2006) noted that “yes” or “no” in situ observations of fire may be difficult to achieve over a very large area and this could not be useful in validation of active fires and hence the remotely sensed fire products such as MODIS can be used.

Morisette et al., (2005) noted that a standard way of assessing the accuracy of remotely sensed data is through the use of an error matrix. The error matrix helps to calculate the overall accuracy and classification accuracy of each class (commission errors (user’s accuracy) and omission errors (producer’s accuracy). Powell et al., (2004) clearly pointed out that it is very important to include a statistically rigorous accuracy assessment with detailed methods so that it could be possible for comparison between the classification techniques or algorithms. There are three methods that are used for the comparison of classifier or algorithm performance: Kappa z-test by Cohen, (1960), Fleiss et al., (1969), MacNemar’s test by McNemar (1947) and Randomization test. De Leeuw et al., (2006) recommended the use of MacNemar’s test when comparing the performance of different methods of classifying maps because it is parametric and extremely simple to understand and execute as compared to other methods mentioned above.

3. Materials and Methods

This chapter gives a brief description of the study area and a detailed outline of the methodology applied in this study.

3.1. Study area

This study is based on two study areas: Portugal and Southern Africa. This was a strategic way of developing and validating the multi-temporal algorithm in different places in terms of scale and environmental or climate conditions.

3.1.1. Portugal

Portugal (Figure 3.1) is mainly characterized by Mediterranean climate which have hot dry summers and cool wet winters. The mean annual temperature is about 18^0C in the south to 7^0C at high altitude to the north and the annual precipitation ranges from about 400 mm to 2 800mm (IA 2003 in Catry et al., (2007 (b)). Fire season in Portugal is normally during the summer months (June to September) and these fires are induced by high temperatures as well as low rainfall which lead to dry conditions which are favourable for occurrence of fires. The Mediterranean climate in Portugal is mainly characterized by highly combustible tree species such as eucalyptus and pine (Gomes, 2006).

The forest fires in Portugal have increased in the last two decades as compared to other southern Mediterranean countries such as Greece, Italy, Spain and France (EC 2005 and DGRF 2006 in Caltry et al., (2007 (a)). It is estimated that about 2.5 million hectares were burned between 1990 and 2005 which is representing 25% of the country area (DGRF 2006 in Caltry et al., (2007 (a)). The problem of forest fires in Portugal is mainly increased by the practicing of the ancient traditional farming methods such as the use of fires to prepare land for new crops, to eliminate waste and to promote growing of grass for cattle feed stock (Gomes, 2006).

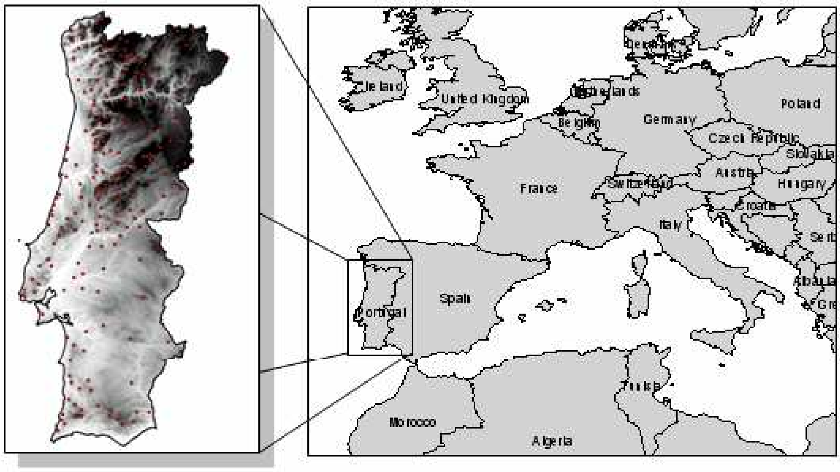

Figure 3.1 Study area (Portugal mainland, with representation of elevation and lookout towers belonging to the NLTN (red points)) (Catry et al., 2007 (b)).

Portugal has a National Lookout Towers Network (NLTN) organised for fire detection system working together with some ground and aerial mobile units. Catry et al., (2007 (b)) evaluated the effectiveness of this system and they concluded that it only detects well fires in 17% of Portugal mainland and is more efficient during the day as compared to night time. This means that there is need for more methods such as remote sensing to supplement this system to reduce the effects of forest fires. However Portugal has an up-to-date forest fire database (Continental Portugal wildfire database) in the custody of Direcção Geral dos Recursos Florestais (DGRF)-Portuguese forest service. The Continental Portugal wildfire database is available online on Ministry of Agriculture website: http://www.afn.min-agricultura.pt/portal/dudf/estatisticas/estatisticas-1996-2006-por-freguesia. This dataset relies on in situ information provided by the Ministry of Agriculture and Civil Protection (Pereira et al., 2007). This database is used in this study for the calibration and validation of the multi-temporal threshold algorithm before it is tested at regional scale in Southern Africa where there is no reliable fire database.

3.1.2. Southern Africa

Africa Southern Africa (Figure 3.2) is greatly affected by forest fires which are ignited by people mainly for land management and by lightning. This occurs during dry season approximately May to October. During this time of the year the herbaceous vegetation is either dry or dormant and the deciduous trees also shed their leaves and these provide fire fuel that is easily combustible. Alleaume et al.,

(2005) noted that under the context of IPCC the estimation of biomass burning and aerosol and trace gas emissions for southern Africa are active areas of research. This can be difficult to achieve without the effective and efficient operational system for near real time active fire detection and monitoring in this region. The most important part in the process of understanding the effects of fire on the atmosphere is to have accurate and reliable information on the time and location of forest fires (Morisette et al., 2005).This is one of the problems in southern Africa as there is lack of ground information on the time and location of fires in this region. Local fire information exists for some areas such as national parks, protected forests and conservation areas especially near the cities. This is however, not representative of the whole region because these areas are under specific conservation management strategies and strictly protected from the influence of people (Roy et al., 2005). Working on Fire (WoF) organisation has a database on fires in South Africa. This organisation is a South African, government-funded, multi-partner organisation which is focused on Integrated Fire Management and wild fire fighting (WoF, 2008). However this organisation does not record all the fires as they consider only big fires which they give much attention mostly near cites. Therefore this gives a biased fire database which is difficult and inappropriate to use in validating forest fire products from remote sensing.

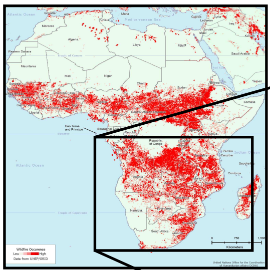

Fires in Africa: 1997-2005.
Source: (ROCEA, 2007)

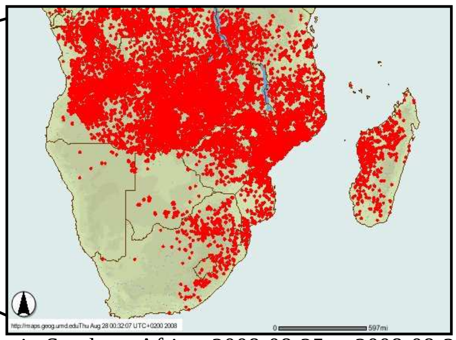

Fires in Southern Africa: 2008-08-25 to 2008-08-27
Source: (FIRMS, 2008)

Figure 3.2 Study area (Southern Africa)

Southern Africa is characterized by three major climatic regions: wet, semi-arid and arid regions. Rainfall distribution in these regions, determines the prevalence or occurrence of fires. In wet regions with rainfall above 1000 – 1200mm/yr there are closed plant canopies and prolonged moist conditions which limit the spread of fires (Roy et al., 2005). The semi-arid regions are mostly affected by fires as they are characterized by woodland savanna and they receive rainfall of about 550 – 750mm/yr. The arid areas (west and southwest interior) receive rainfall of less than 550mm/yr and the vegetation is mainly shrubs and grass production is determined by the annual rainfall therefore fires are normally intermittent and normally follow the periods of well above average rainfall (Roy et al., 2005).

There are many research and development organizations which are working on fire in southern Africa and these include International Southern African Regional Science Initiative (SAFARI) - 2000, Regional Sub-Saharan Wildland Fire Network (Afrifirenet) and the Southern African Fire Network (SAFNET). Afrifirenet developed the South African Advanced Fire Information System (AFIS) which is one of the first near real time satellite based fire monitoring system in Africa (Frost and Scholes, 2007). The Fire Information for Resource Management System (FIRMS) developed at the University of Maryland is also providing MODIS active fire data to natural resource managers, scientists and policy managers in 58 countries (Groot et al., 2007) and these include those in southern Africa. However there is need to augment these efforts by developing a fire detection system that is as near real time as possible so as to be able to reduce the effects of fire on human beings health and safety, regional economies, global climate change and fire sensitive ecosystems.

3.2. Data used

MSG SEVIRI satellite data (including the images, MPEF cloud mask (CLM) and FIR-G - fire product) was used for the development of the near-real time active fire detection algorithm in this study. The MSG images were downloaded from the 3 years MSG archive at ITC using MSG data retriever. The other MSG products (MPEF cloud mask (CLM) and FIR-G) were obtained from EUMETSAT. The ground truth data for validation of the algorithm was obtained from Portugal (Ministry of Agriculture: http://www.afn.min-agricultura.pt/portal/ dudf/estatisticas/ estatisticas-1996-2006-por-freguesia). At the time of this study this database was updated to 2006 and the data for 2007 was directly obtained from Portuguese Ministry of Agriculture. The fire database obtained from Working on Fire (WoF) organisation had no spatial coordinates which made it difficult to use in validating the algorithm. Therefore for Southern Africa the MODIS fire product (ftp://e4ftl01u.ecs.nasa.gov/) was used in the validation of the multi-temporal threshold algorithm developed in this study. The MPEF fire product (FIR-G) was used for comparison with the algorithm developed in this study with reference to ground fire data from Portugal and MODIS fire product. The MPEF fire product

(FIR-G) was chosen as it is also based on MSG so there are no problems with spatial and temporal resolution.

3.3. Data processing and analysis

3.3.1. Pre-processing of data

(i) Geometric calibration of MSG images

The geometric calibration of MSG images is done in the MSG data retriever developed at ITC. The pixel position (x,y) in the image corresponds to angles in x and y direction because of the scanning characteristics of the SEVIRI instrument (Gieske et al., 2005).

(ii) Radiometric calibration of MSG images

This is the conversion of DN values to radiance and further to the brightness temperatures. This is also done using MSG data retriever. The DN values are converted to DN values by:

$$R = slope * DN + offset$$

Where R is the radiance [$(mWm^{-2}sr^{-1}(cm^{-1})^{-1}$]. Slope and offset are obtained from the header file and DN refers to the digital numbers from the satellite. In this study the brightness temperatures (top of the atmosphere) in channel 3.9µm and 10.8µm channels are going to be used and the following equation is used to convert the radiance to brightness temperatures in MSG data retriever.

$$T_b = \left[c_2 \nu_c \Big/ \log\left(c_1 \nu_c^{\,3} \big/ R + 1 \right) - B \right] \Big/ A$$

Where T_b is the brightness temperatures (K); R is the radiance [$(mWm^{-2}sr^{-1}(cm^{-1})^{-1}$]; ν_c is the central wave number of the channel for constants; $c_1=2hc^2$ and $c_2=hc/k_B$ are the radiation constants; c is the velocity of light, k_B is Boltzmann's constant and h is Planck's constant; A and B are the band constants from the header file (Gieske et al., 2005). The values for the parameters in the equation above are shown in Appendix 1.

(iii) Processing of ground data

The ground data from Portugal was used to develop and validate the algorithm before it was applied to Southern Africa. This is because actual ground fire data is not well documented in most of the Southern African countries. The ground data (fire points) from Portugal was obtained from the Department of Agriculture and Forestry (Portugal). The most important information recorded in this database which was required in this study include: (i) date (ii) time the fire started (iii) extinction time (iv) burned area (v) spatial coordinates. This data was in x and y coordinates Transverse Mercator projection and GCS_Datum_Lisboa Hayford geographic coordinate system. These points were re-projected to lat/long WGS 84 and then changed to the same projection and coordinate system with the MSG images. The dates and time for the actual fire ground data from Portugal are shown in the table below:

Table 3.1 Portugal ground fire data (obtained from fire database)

Date	Time UTC	
	From	To
21/08/05	0000	2345
06/09/07	0000	2345
07/09/07	0000	2345

The ground data for 21 August 2005 was used for the development and calibration of the algorithm. Other ground fire data sets were used for the validation of the algorithm. These dates were selected considering different sizes of fires (in terms of burned areas) to check if the algorithm could also detect very small fires. The fire points were sorted according to time steps of 15 minutes so that they go hand in hand with the temporal resolution of MSG satellite. The time on the databases was recorded in local time (UTC+1 hour), so to match with MSG images, it was converted to UTC.

(iv) Processing of the MSG FIRG product, Cloud mask and MODIS fire product

These products were processed differently as described below, but they were all set to the same MSG georeference system to make it easier and appropriate for comparison and validation of the fire products.

(a) MSG FIR-G product

This product was obtained from EUMETSAT as a full disk MSG image in GRIB (Gridded Binary) file format. This was changed to boolean map in ILWIS format showing fire and no fire. This was then converted to a vector map which shows the fire polygons to be compared with the results of the multi-temporal algorithm developed in this study.

(b) Cloud mask

The cloud mask was obtained from EUMETSAT in full pixel resolution displaying information on the presence of clouds. This was also obtained as full disk image in GRIB (Gridded Binary) file format and was converted to ILWIS file format and resampled to the specific areas of interest (Portugal and Southern Africa).

(c) MODIS fire product

MODIS fire products (MOD14 (Terra) and MYD14 (Aqua) were downloaded from MODIS site: ftp://e4ftl01u.ecs.nasa.gov/ as hdf (hierarchical data format) files. These files were converted to shapefiles using mod142shp tool that is a utility to extracts MOD14 fire pixel locations and store them in ESRI SHP vector map file as points. These points or shapefiles were later imported into ILWIS software. Only those files with the overpass time that coincided with MSG over the study areas (Portugal and Southern Africa) for the dates in table 5 above were considered in this study.

3.3.2. Development of the system for active fire detection

The development of the system for active fire detection using geostationary satellites in this study required three major steps: development of the algorithm, validation and the automation of the procedures. These steps are shown in figure 3.3 below:

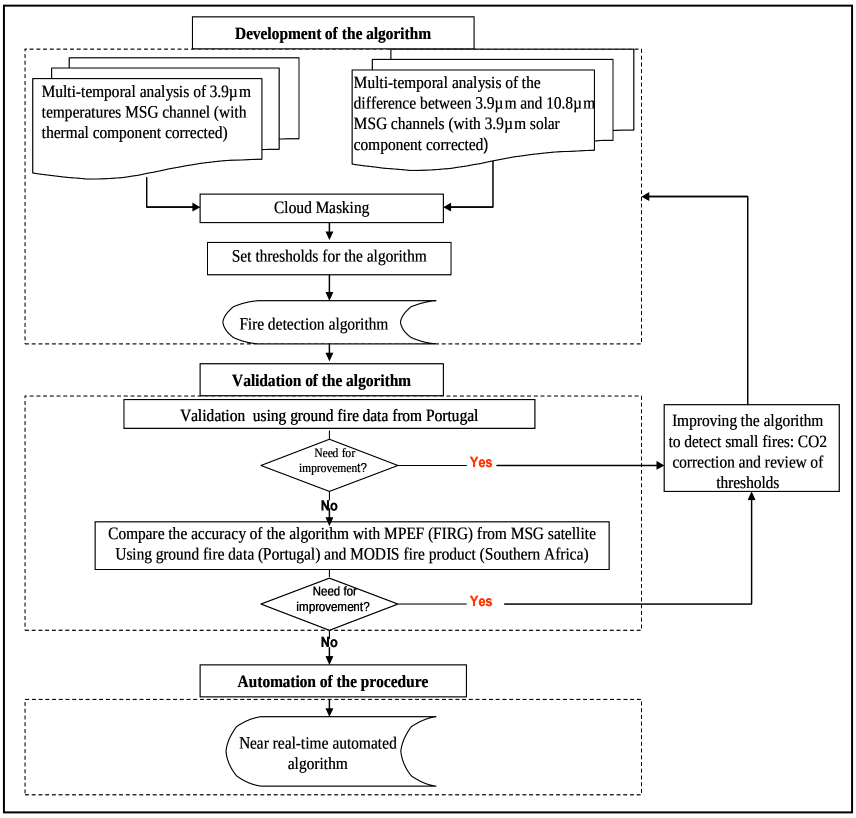

Figure 3.3 An overview of the steps in developing the active fire detection system

3.3.2.1. Development of the multi-temporal threshold algorithm

The development of the algorithm involved three major activities: cloud masking, multi-temporal analysis of 3.9µm temperatures and the difference between 3.9µm and 10.8µm temperatures and setting the thresholds for fire detecting algorithm. The data for 21 August 2005 was used for the development and calibration of the algorithm. Since the MODIS fire product was also used in this process the specific times which coincided with MODIS (both Aqua and Terra sensors) overpass were considered and these are: 12:00, 23:00, 01:30 and 02:25 UTC.

(i) Cloud masking

This method is ideal for cloud free days. It is nearly impossible to have 9 consecutive cloud free days for all the pixels over a large area; therefore a cloud mask was applied on all the images. MSG MPEF system provides the cloud mask for every image so this is used to mask out all the areas covered by clouds so that they will not influence the results. There are some transparent clouds such as cirrus which are difficult to detect and remove and may lower the temperatures in IR3.9 and this may bring bias in the analysis and results. In multi-temporal analysis not only clouds can disturb but also the fires which may have occurred in the previous days can raise the mean (background) temperature and some fires can me missed. Therefore random sampling was done to pick the pixels from the image for 15 September 2007 and multi-temporal analysis was done to check the variation of temperatures after cloud removal. It was realised that the temperature was -3 and $+3^0$ K around the mean temperature. Based on this finding all the days with pixels with temperature below -3 and beyond $+3^0$ K were not included in the analysis to get approximate normal background temperature. The cloud mask is also applied on the 10^{th} image to remove the pixels contaminated by clouds.

(ii) Multi-temporal analysis

The multi-temporal analysis was done to detect the temperature anomalies on the MSG SEVERI images. Temperature anomalies are signals to show the possibility of active fires (hot spots) as the fires produce a local increase of temperatures above the normal background temperatures. The approach is more or less similar to a multi-temporal robust satellite technique for forest fire detection by Mazoo et al., (2007) as it is based on change detection scheme that detects signal anomalies by utilizing the spatio-temporal domain of the geostationary satellites. This is basically realized on the deviations from normal state of the environment that has been preliminarily identified. Koltunov and Ustin, (2007) noted that the multi-temporal approach defines fires as a class of anomalous changes in the scene. The analysis was done using the 3.9µm (sensitive to temperature changes) and 10.8µm (less sensitive to temperature changes) channels.

The choice of the number of past images is also important and a minimum of 8 is recommended for anomaly detection (Koltunov and Ustin, 2007). In this study 10 images of consecutive days of the same time of the day were used to detect the temperature anomalies. Out of these 9 images only the non-anomalous days were used for each pixel. It was realized that each pixel had a different number of non-anomalous (in terms of temperature) days which varied from 0 to 9 and therefore only those pixels with more than two days cloud non-anomalous days were included in the analysis. It was assumed that with at least 3 non-anomalous days the approximate normal temperatures can be estimated. The average temperature for each pixel was calculated using the formula below:

$$m_{t(3.9\mu m)} = \frac{\sum dT_{3.9\mu m(i)}}{N}$$

Where $m_{t(3.9\mu m)}$ is mean temperature for IR3.9 channel for the past anomaly free days (between 3 and 9 days).
N is the number of anomaly free days (between 3 and 9).
$dT_{3.9\mu m(i)}$ is the temperature of the day at the same time at 3.9µm.

Figures 3.4 and 3.5 below show the maximum and minimum number of days included in the analysis to estimate the background temperatures without the anomalies.

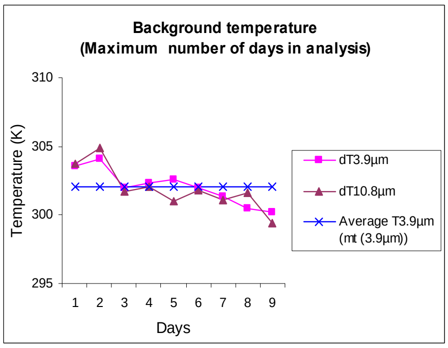

Figure 3.4 Background temperature (Maximum number of days in analysis)

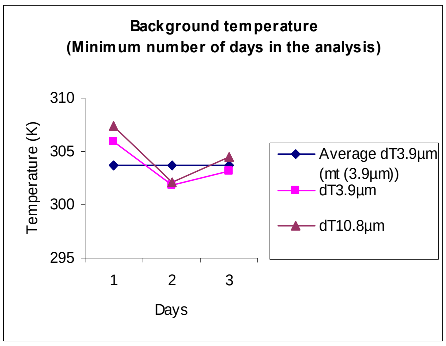

Figure 3.5 Background temperature (Minimum number of days in analysis)

If the temperature of the day at that particular time is higher than the mean temperature it means that there is a temperature anomaly and there is a possibility of fire. However the thresholds are set in section 3.3.2 (iii) below.

The brightness temperature of IR10.8 is normally lower as compared to the brightness temperature in channel IR3.9 (EUMETSAT, 2007). The difference between the temperatures in the two channels is also used to detect hot spots. There is a higher difference on fire than non-fire pixels. In this study, the difference (on the same time same day) is calculated as shown below:

$$T_{dif} = dT_{3.9\mu\mathrm{m(i)}} - dT_{10.8\mu\mathrm{m(i)}}$$

Where T_{dif} is the difference in temperature between IR3.9 and IR10.8 channels
$dT_{3.9\mu m(i)}$ is the temperature of the day at the same time at 3.9µm.
$dT_{10.8\mu m(i)}$ is the temperature of the day at the same time at 10.8µm.

This is applied to all the images and the average difference is obtained using the formula:

$$\mathrm{m}_{\mathrm{dif}} = \frac{\sum T_{\mathrm{dif(i)}}}{\mathrm{N}}$$

Where m_{dif} is the mean of the differences in temperatures in IR3.9 and IR10.8 channels for the past anomaly free days (between 3 and 9 days).
N is number of anomaly free days (between 3 and 9).
$T_{dif\ (i)}$ is the difference in temperature between IR3.9 and IR10.8 channels

Figures 3.6 and 3.7 below show the maximum and minimum number of days included in the analysis to estimate the difference between IR3.9 and IR10.8 temperatures without the anomalies.

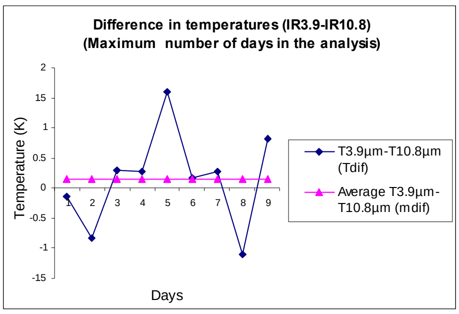

Figure 3.6 Background temperature (difference in IR3.9 and IR10.8 channels)

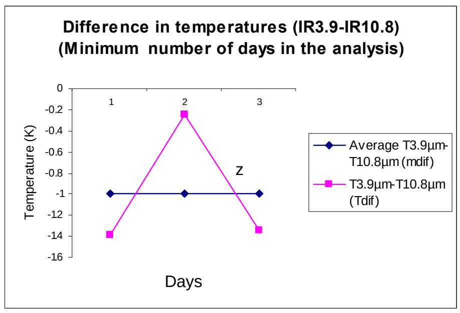

Figure 3.7 Background temperature (difference in IR3.9 and IR10.8 channels)

Temperature anomalies are realized if the difference in temperature between channel IR3.9 and IR10.8 is above the mean difference temperature. The pixels on the image have different number of anomaly free days to be included in the analysis to get the approximate mean difference in IR3.9 and IR10.8 background temperatures. Therefore the number of anomaly free days (N) varies from 0 – 9 days. Only those pixels with N greater than 2 are considered in the analysis. It was noted that the number of pixels with N less than or equal to two (2) varies each time since clouds are also highly dynamic environmental phenomenon. Figure 3.8 below is an example which shows the number of pixels with different number of anomaly free days at 0230 UTC (21 August 2005).

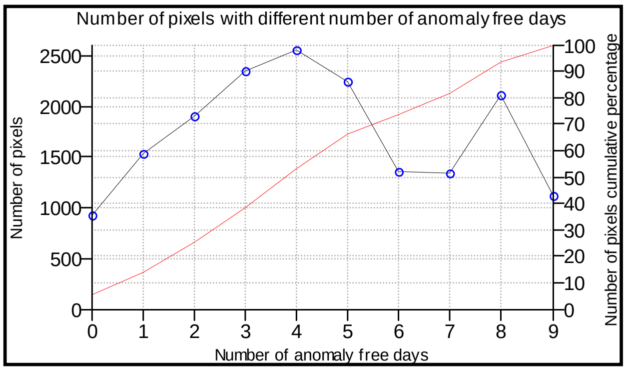

Figure 3.8 Pixels with different number of anomaly free days (21 August 2005 (0230 UTC))

From figure 3.8 above the number of pixels with anomaly free days (N) less than or equal to two (2) is 25%. By eliminating these pixels it helps to have confidence in the final result as it could be difficult to rely on background temperature estimated using the temperatures observed in only 2 days or less. This reduces the false fire alarms but some fires maybe missed as well, however, clouds are a rapidly changing environmental phenomenon and considering the temporal resolution of MSG (15 minutes) the fires missed may be detected on subsequent time steps.

(iii) Thresholds for fire detection

In addition to the mean temperatures for IR3.9 and IR3.9-IR10; the standard deviation (for IR3.9 and IR3.9-IR10.8) was also required to determine the thresholds for the algorithm. The standard deviation for IR3.9 channel was calculated using the following formula:

$$S_{t\,(3.9\mu m)} = \sqrt{\frac{\sum (dT_{3.9\mu m\,(i)} - m_{t(3.9\mu m)})^2}{N}}$$

Where S_t is the standard deviation temperature in IR3.9 for the past anomaly free days (between 3 and 9 days).

$m_{t\,(3.9\mu m)}$ is the mean temperature.

N is the number of anomaly free days (between 3 and 9).

$dT_{3.9\mu m\,(i)}$ is the temperature of each day at the same time at 3.9µm.

The standard deviation for the differences between IR3.9 and IR10.8 is also calculated.

$$S_{dif} = \sqrt{\frac{\sum (T_{dif\,(i)} - m_{dif})^2}{N}}$$

Where S_{dif} is the standard deviation of the differences in temperature for the past anomaly free days (between 3 and 9 days).

m_{dif} is the mean of the differences in temperatures for the past ten days.

N is the number of anomaly free days (between 3 and 9)

T_{dif} is the difference in temperature between IR3.9 and IR10.8 channels for each day at the same time.

The thresholds can be determined using the S_t and S_{dif} together with the averages calculated in 3.3.2 (ii) above (m_t and m_{dif}) and f value as explained below. For the hot spot to be classified as actual fire it should meet the following specifications:

$$dT_{3.9\mu m} > m_{t(3.9\mu m)} + f_1(S_{t(3.9\mu m)})$$
$$T_{dif} > m_{dif} + f_2\,(S_{dif})$$

The hot spot may be classified as possible fire if:

$$dT_{3.9\mu m} > m_{t(3.9\mu m)} + f_3(S_{t(3.9\mu m)}) < m_{t(3.9\mu m)} + f_1(S_{t(3.9\mu m)})$$
$$T_{dif} > m_{dif} + f_4(S_{dif}) < m_{dif} + f_2(S_{dif})$$

The f value is the most critical factor in the above specifications as it determines the level of the thresholds. The specifications for actual fires and possible fires are different because the actual fires take the highest values from the approximate normal background temperatures while the possible fires take the values between the normal background temperatures and the actual fires. This is all determined by the *f* values in the algorithm.

However the IR3.9 channel records the reflected energy from the sun and Earth's radiant energy during the day (Figure 2.3) and during the night it records the energy from the earth only. This means that this channel has different responses during the day and so *f* was different for day and night thresholds. The day images are defined by the solar zenith angle of less than 70^0 and night for the solar zenith > 90^0 for the angles between 70^0 and 90^0 the thresholds are linearly interpolated (Appendix 4) (EUMETSAT, 2007). Several tests were done to get the appropriate *f* values by using the error matrix to get the values with the highest accuracy (Appendix 2 and 3). In determining the *f* values all the fires in the database for the particular times (0230 UTC and 1200 UTC 21 August 2005 in Portugal) were considered. The histogram below shows the fires used in determining the *f* values for the thresholds.

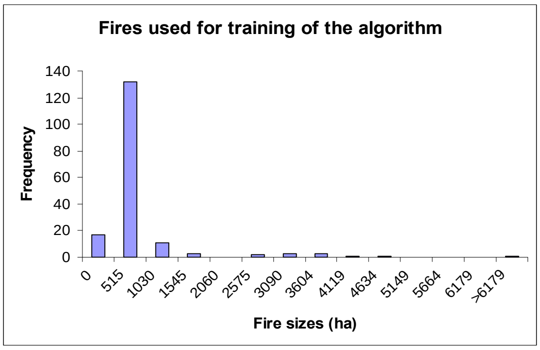

Figure 3.9 Fires used for development and training of the algorithm

(iv) CO_2 absorption correction

With reference to figure 2.6 it can be noted that records in IR3.9 channel (spectral range 3.48 to 4.36µm) are greatly affected by CO_2 absorption. Therefore correction for carbon dioxide absorption was also done to assess if this can improve the performance of the algorithm. A method suggested by Rosenfeld (2005) was used to correct for CO_2 absorption.

$$T4\_CO2corr = (BT\ (IR3.9)^{4} + Rcorr\ )^{0.25}$$

Where:

T4_CO2corr, the CO2-corrected brightness temperature (BT) at IR3.9,

$$Rcorr = BT\ (IR10.8)^4 - (BT\ (IR10.8) - \Delta T\_CO2)^4$$

$$\Delta T\_CO2 = (BT\ (IR10.8) - BT\ (IR13.4))\ /\ 4$$

The CO2 – correction of brightness temperature (BT) in IR3.9 depends non-linearly on ΔT_CO2, the difference IR10.8 and IR13.4, which depends on:

- Temperature difference between surface and air mass at about 850 hPa (ΔT_CO2 is very large for hot desert surfaces during day time)
- Height of cloud (ΔT_CO2 is small for high clouds)
- Satellite viewing angle (so-called “limb cooling” effect, ΔT_CO2 is large for large satellite viewing angles)
- Differences in surface emissivity at 10.8 and 13.4 µm

(Rosenfield, 2005)

CO_2 correction raises the temperatures in IR3.9 channel so the thresholds were also changed and evaluated using the same method explained in 3.3.2 (a) (iii) above (Appendix 6 and 7) and the accuracy was assessed as explained in 3.3.2 (b) below.

3.3.2.2. Validation of the algorithm

After development and training of the algorithm validation was done using ground data from Portugal and the MODIS fire product (Portugal and Southern Africa).

Sampling design is a critical part of the validation process as it determines the quality of results and makes the algorithm comparable with other algorithms for fire detection. Simple random sampling is the most recommended design as it gives every pixel equal chances of being selected and one of its advantages is simplicity (Stehman, 1999). However (Longley et al., 2005) pointed out that in some cases some classes are more common than others and a random sample that gives the equal probability for every parcel or pixel to be chosen may be inefficient as too many data may be gathered on common classes and not enough for the relatively rare classes. This was also considered in this study as the hotspots which indicate fires may not be common as compared to the non-fire areas. Therefore simple random sampling is not applicable in this study. The fire pixels from the satellite (algorithm and MPEF-FIRG) were compared with fire areas or points from the ground data. Non-fire areas were not considered when assessing the accuracy of each method with reference to ground data as they may bring bias in the accuracy level of the algorithm. The structure of the error matrix used is shown below:

Table 3.2: Error matrix

Fire Ground data

	Fire	Y	N	Total
	Y			
Fire Map	N			
	Total			

Y = Fire
N = No fire

The fire ground data from Portugal was used in the validation of the maps obtained through the use of the algorithm developed in 3.3.2 (a) above. The error matrix was used to calculate the commission (user's accuracy) and omission errors (producer's accuracy). Sensitivity analysis was performed (0230, 1200, 1330 and 2300 UTC (21 August 2005) in Portugal) to determine the fire size levels at which the algorithm can detect 50% of the fires and above. The sizes of fires are based on the fraction of the pixel covered by fire (Figure 2.5) given the MSG spatial resolution of 3km (900 hectares). The table below shows the sizes of fires used in the sensitivity analysis.

Table 3.3 Sizes of fires used in sensitivity analysis

Fraction of a pixel covered by fire	Area burned (ha)
0.025	22.5
0.050	45.0
0.075	67.5
0.100	90.0
0.125	112.5
0.150	135.0
0.175	157.5
0.200	180.0

As the fraction of the pixel covered by fire increases there will be more deviation from the approximate normal background temperature (Figure 2.5) and this may also increase the fire detection rate of the algorithm.

As recommended by Foody, (2004) and de Leeuw et al., (2006) the McNemar's test (1947) was used to test the hypothesis of this study. This method was used to compare the performance of the multi-temporal threshold algorithm developed in this study and the MPEF FIRG product from MSG satellite. This was also used to compare the performance of two algorithms developed in this study:

(i) Algorithm A - developed without the removal of the solar constant and CO_2 absorption

(ii) Algorithm B - developed with the removal of both solar constant and CO_2 absorption.

McNemar's test is based on 2 x 2 matrix as shown in table 3.4 below. The null hypothesis is that both algorithms under investigation have the same performance on detecting fires. When using the McNemar's test the frequency table includes the no fire pixels since it is a comparison of two methods and these no fire pixels may be wrongly detected as fires by another algorithm.

Table 3.4 Cross tabulation of number of correct and wrongly classified pixels for two algorithms

Algorithm A	Algorithm B	
	Wrong	Correct
Wrong	f_{11}	f_{12}
Correct	f_{21}	f_{22}

The method uses a population ratio:

$$\psi = \hat{f}_{12} / \hat{f}_{21}$$

This is estimated by the simple ratio f_{12} / f_{21} thus the null hypothesis equals H_o: $\psi = 1$. The method is based on the chi-square statistic that is computed as shown below:

$$x^2 = (f_{12} - f_{21})^2 / (f_{12} + f_{21})$$

The P-value of the McNemar's test is then used to reject or not reject the null hypothesis of equal algorithm performance. With reference to the x^2 test tables, the null hypothesis is rejected if the x^2 result is significant (p-value<0.05) with the degree of freedom (df) of 1.

The data used for the validation of the algorithm is independent of the data used in developing this algorithm. This was done to avoid biased accuracy assessment of the algorithm. The times considered for validation and comparison of the performance of the algorithms are shown in Appendix 8. As for Southern Africa the MODIS fire product for 06 September 2007 at 1215 UTC was considered for the comparison of MSG fire product and the multi-temporal algorithm developed in this study. The frequencies obtained on the comparison of the different methods or algorithms as well the error matrices for the individual algorithms are shown in Appendix 9-12.

3.3.2.3. Automation of the procedure for the algorithm

The procedure for the active fire detection multi-temporal algorithm described above is summarised in the flow diagram below.

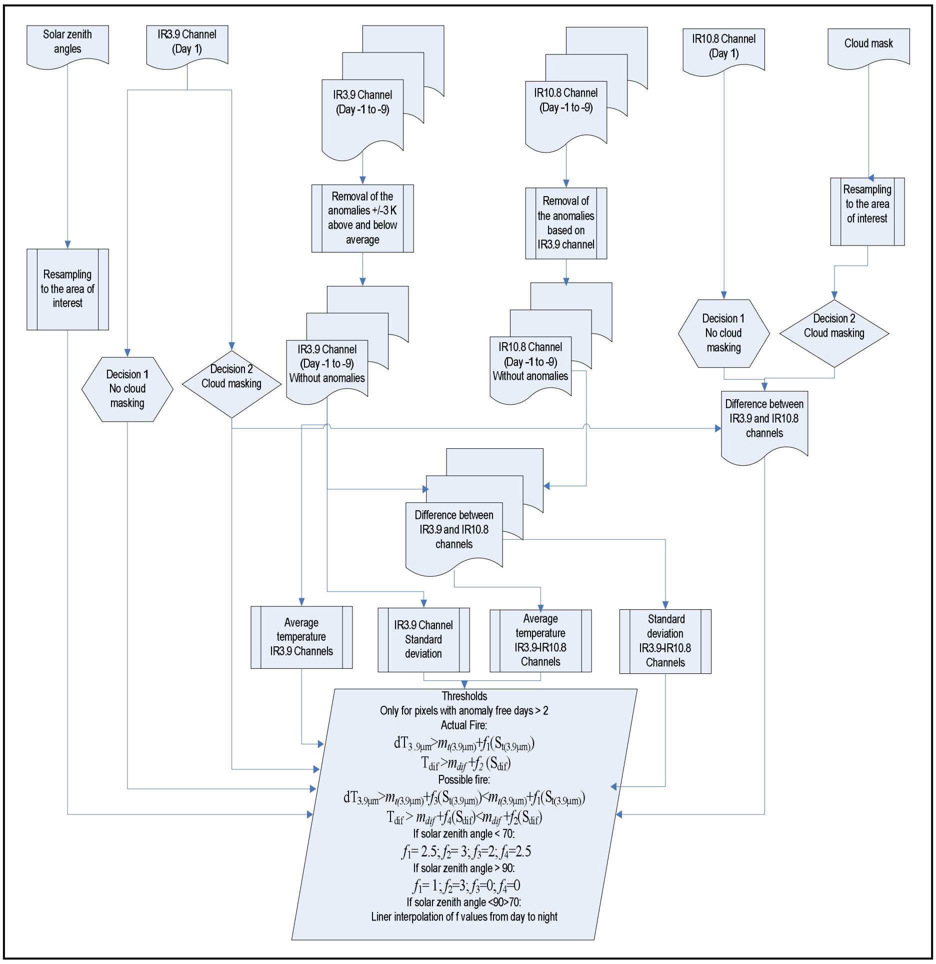

Figure 3.10 Procedure for the algorithm

The procedure was automated using ILWIS software. The exact operations of what is done at each and every step in figure 3.10 above are shown in the scripts in Appendix 13-16.

4. Results

This chapter outlines the results obtained from the methods outlined in chapter 3 and it focuses on the multi-temporal threshold algorithm, accuracy of the multi-temporal threshold algorithm and the automated procedure of the algorithm.

4.1. Multi-temporal threshold algorithm

The algorithm is based on the multi-temporal thresholds developed on the basis of temperature anomalies detected in IR3.9 channel and the difference between IR3.9 and IR10.8 MSG channels over a period of consecutive days.

4.1.1. Temperature anomalies

The temperature anomalies can be detected using IR3.9 channel (Figure 4.1) and the difference between IR3.9 and IR10.8 channels (Figure 4.2).

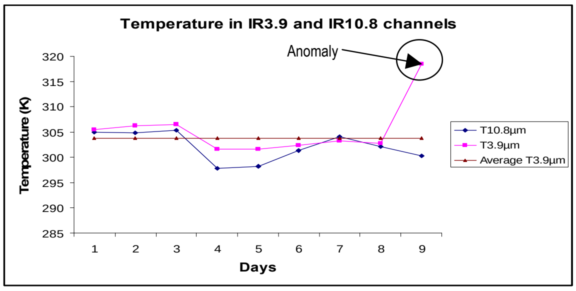

Figure 4.1 Temperature anomaly in IR3.9 channel

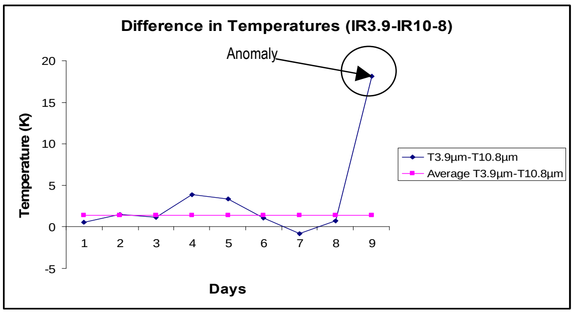

Figure 4.2 Temperature anomaly (difference between IR3.9 and IR10.8 channels)

The anomalies are observed as there is a deviation from the average (normal) background temperatures. Since the number of anomaly free days (N) varies for each pixel on the image, the example used in this case has 8 days included in the analysis to get the approximate background temperature. The difference between IR3.9 and IR10.8 temperatures is important for forest fire detection as the temperature in IR3.9 channel alone may not show the occurrence of fires. In some cases IR3.9 temperatures may be above the mean IR3.9 temperature but there could be no difference between IR3.9 and IR10.8 or the difference is not very high above the mean or average difference. This means that this anomaly is not significant and cannot be attributed to forest fires for example days 1-3 in figures 4.1 and 4.2 above.

4.1.2. Thresholds for the algorithm

IR3.9 channel is sensitive to temperature changes as compared to IR10.8 channel and it also records the solar reflectance at the top of atmosphere. This means that during the day temperatures in IR3.9 are higher than those in IR10.8 channel but since IR3.9 channel is sensitive to temperature changes it can also be lower than IR10.8 due to some anomalies or daily temperature variation (Figure 4.3 below). During night time when there are no anomalies such as fires and clouds, temperatures in IR3.9 are lower than in IR10.8. This is mainly because there is no solar component recorded in IR3.9 channel during night time and this channel is very sensitive to temperature changes (Figure 4.4).

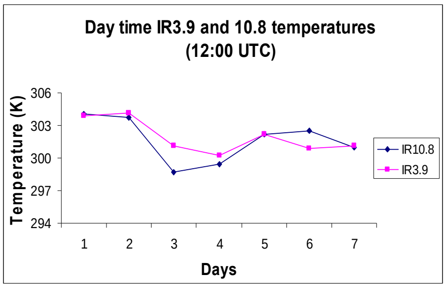

Figure 4.3 Day time IR3.9 and IR10.8 temperatures

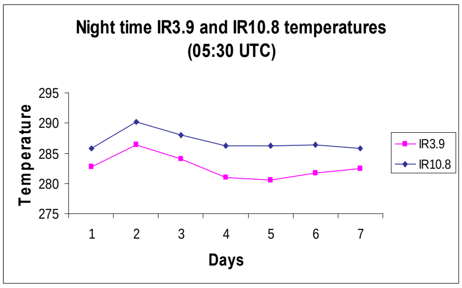

Figure 4.4 Night time IR3.9 and IR10.8 temperatures

Based on the differences in temperatures in IR3.9 channel in relation to IR10.8 channels during the day and night; thresholds for day and night are also different. The thresholds for actual fire and probable fire are shown below:

(i) Actual fire

$$dT_{3.9\mu m} > m_{t(3.9\mu m)} + f_1(S_{t(3.9\mu m)})$$

$$T_{dif} > m_{dif} + f_2\,(S_{dif})$$

(ii) Probable fire

$$dT_{3.9\mu m} > m_{t(3.9\mu m)} + f_3(S_{t(3.9\mu m)}) < m_{t(3.9\mu m)} + f_1(S_{t(3.9\mu m)})$$

$$T_{dif} > m_{dif} + f_4(S_{dif}) < m_{dif} + f_2(S_{dif})$$

Day time $f_1 = 2.5$; $f_2 = 3$; $f_3 = 2$; $f_4 = 2.5$; Night time $f_1 = 1$; $f_2 = 3$; $f_3 = 0$; $f_4 = 0$

In this algorithm *f* is the most variable factor hence it determines the difference between actual and possible fire during the day and night. The *f* values for the thresholds were determined by the accuracy of different combinations of different *f* values. The *f* values chosen had a higher producer accuracy of 22.1% and 19.2% for day and night respectively (Appendix 2 and 3). For twilight condition the *f* factor is linearly interpolated (Appendix 4). The results of the algorithm during the training and calibration of the method are shown below:

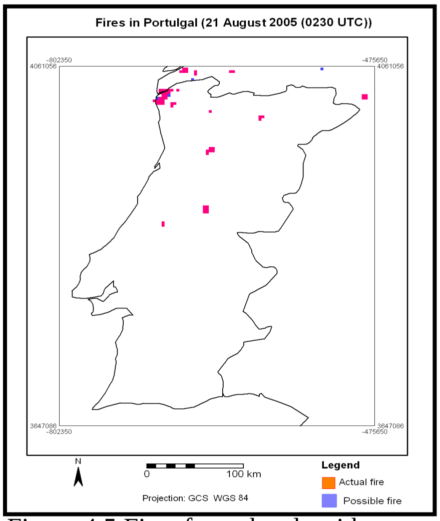

Figure 4.5 Fires from the algorithm during night time

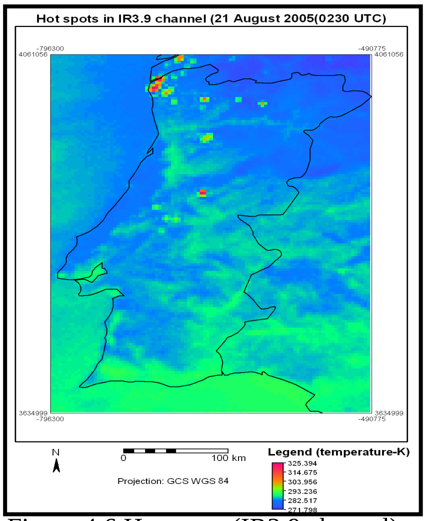

Figure 4.6 Hot spots (IR3.9 channel) night time

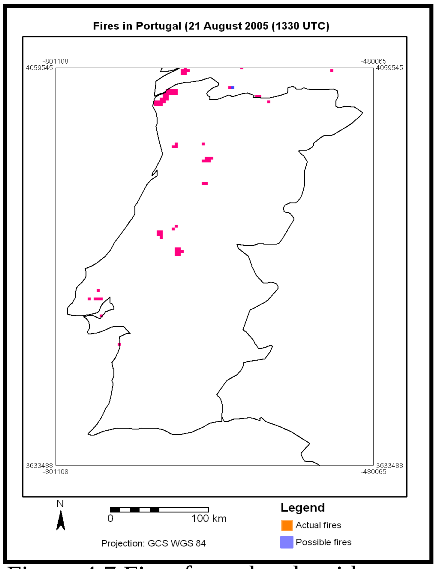

Figure 4.7 Fires from the algorithm during day time

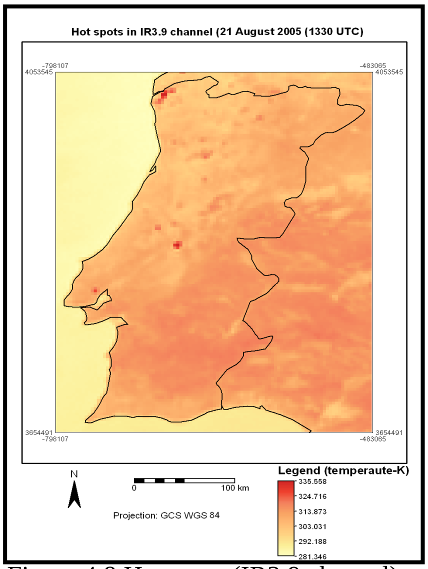

Figure 4.8 Hot spots (IR3.9 channel) during the day

4.2. Validation of the algorithm

4.2.1. Sensitivity analysis

As noted in 4.1.2 above the accuracy of the algorithm was very low as it could not detect all the fires so sensitivity analysis was done to get the threshold at which the algorithm can detect 50% of the fires and above (Appendix 5). Figure 4.9 below shows the levels of accuracy as determined by the sizes of fires.

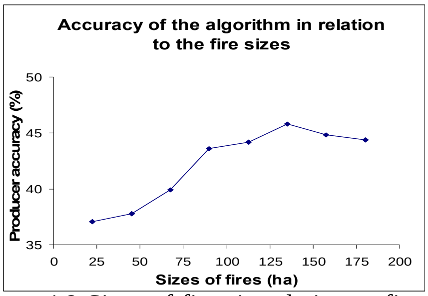

Figure 4.9 Sizes of fires in relation to fire detection levels of the algorithm

The algorithm could not give the producer accuracy of 50%. It obtained the highest producer accuracy of 45.8% when fires of sizes greater than 135 hectares were used for validation. This was considered to be the fire sizes at which the algorithm could attain the highest accuracy and therefore was used in the higher levels of validation of the algorithm. The maps below show the fires (greater than or equal to 135ha) detected by the algorithm.

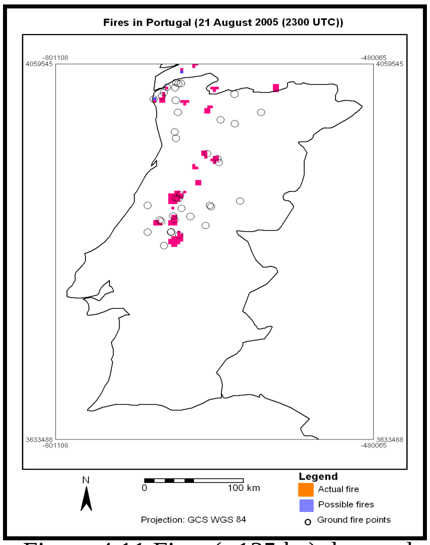

Figure 4.11 Fires (>135 ha) detected by the algorithm (1200 UTC)

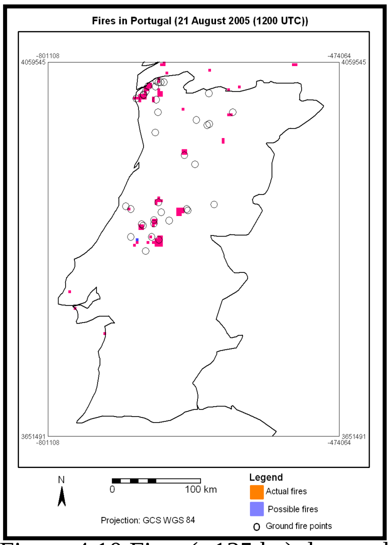

Figure 4.10 Fires (>135 ha) detected by the algorithm (2300 UTC)

4.2.2. Comparison between the algorithm and the MSG FIRG product

The maps below show some of the results of the comparison between multi-temporal threshold algorithm and the contextual algorithm (MSG FIR-G product) using ground data from Portugal.

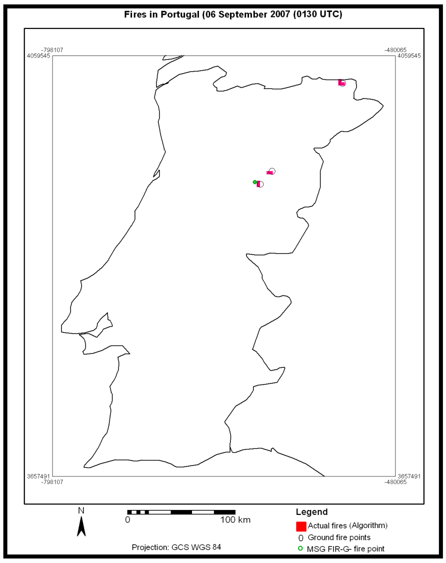

Figure 4.12 Fires (>135 ha) detected by the algorithm and MSG FIR-G product (0130 UTC)

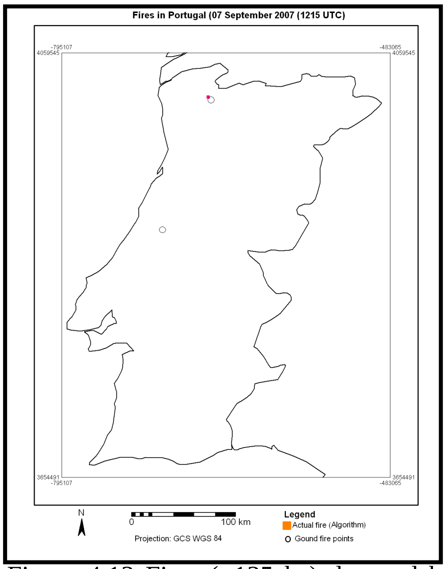

Figure 4.13 Fires (>135 ha) detected by the algorithm and MSG FIR-G product (1215 UTC)

Table 4.1 below shows the accuracy of the multi-temporal threshold algorithm and MSG FIR-G product (contextual algorithm). Table 4.2 shows the comparison of these two algorithms when same ground data set from Portugal fire database was used for validation. These results are based on the error matrices and frequency table for the performance of these algorithms in Appendix 9.

Table 4.1 Accuracy of the algorithms: (multi-temporal threshold algorithm and contextual threshold algorithm (MSG FIRG product)

	Errors of commission (%)	Errors of omission (%)	Fires Detected (%)
Multi-temporal threshold algorithm	20.6	50	50
Contextual algorithm **(**MSG FIRG)	0	96.3	3.7

Table 4.2 Frequency of correct and wrongly classified pixels by the multi-temporal threshold algorithm and contextual algorithm (MSG FIR-G product)

MSG FIRG	Multi-temporal threshold algorithm		Total
	Wrong	Correct	
Wrong	25	22	47
Correct	9	5	14
Total	34	27	61

These results indicate that the multi-temporal threshold algorithm has a higher accuracy compared to the contextual algorithm (MSG FIR-G product); this difference is significant (McNemar's test statistic (x^2) = 5.45, df = 1, p-value = 0.0196) and therefore the null hypothesis of equal performance of these two algorithms is rejected.

4.2.3. CO_2 correction of the IR3.9 channel

4.2.3.1. CO_2 correction and changing of thresholds

The correction of CO_2 absorption in IR3.9 channel raises the temperatures in this channel as shown in figure 4.14 below:

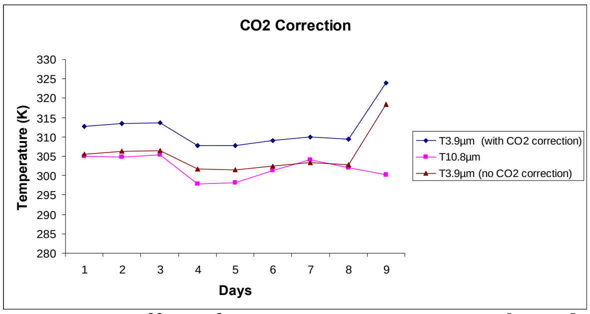

Figure 4.14 Effect of CO_2 correction on IR3.9 channel

As the temperature in IR3.9 channel increases due to the correction of CO_2 absorption the thresholds for actual fire and probable fire were also changed to the ones shown below (see also Appendix 6 and 7):

(i) Actual fire

$$dT_{3.9\mu m} > m_{t(3.9\mu m)} + f_1(S_{t(3.9\mu m)})$$

$$T_{dif} > m_{dif} + f_2\,(S_{dif})$$

(iii) Probable fire

$$dT_{3.9\mu m} > m_{t(3.9\mu m)} + f_3(S_{t(3.9\mu m)}) < m_{t(3.9\mu m)} + f_1(S_{t(3.9\mu m)})$$

$$T_{dif} > m_{dif} + f_4(S_{dif}) < m_{dif} + f_2(S_{dif})$$

Day time f_1= 2.5; f_2= 3; f_3=2; f_4=2.5; Night time f_1=6; f_2=7.5; f_3=5.5; f_4=5.5

4.2.3.2. Comparison of the algorithms: without CO_2 correction and with CO_2 correction

Table 4.3 below shows the accuracy of the two multi-temporal threshold algorithms; i) with CO_2 correction and ii) without CO_2 correction. Table 4.4 shows the comparison of these two algorithms when same ground data set from Portugal fire database was used for accuracy assessment. These tables are based on the error matrices and frequency table in Appendix 10.

Table 4.3 Accuracy of the algorithms: (multi-temporal threshold algorithms (without CO_2 correction and one with CO_2 correction)

	Errors of commission (%)	Errors of omission (%)	Fires Detected (%)
Multi-temporal threshold algorithm without CO_2 correction	38.5	48.4	51.6
Multi-temporal threshold algorithm with CO_2 correction	85.6	51.6	48.4

Table 4.4 Frequency of correct and wrongly classified pixels by the multi-temporal threshold algorithms (without CO_2 correction and one with CO_2 correction)

Multi-temporal threshold algorithm with CO_2 correction	Multi-temporal threshold algorithm without CO_2 correction		Total
	Wrong	Correct	
Wrong	27	184	211
Correct	23	27	50
Total	50	211	261

There is a difference between the performance of the two multi-temporal threshold algorithms; with CO_2 correction and without CO_2 correction. The multi-temporal threshold algorithm without CO_2 correction correctly classified more fire points which where misclassified by the multi-temporal threshold algorithm with CO_2 correction. The difference between the performances of the two algorithms is significant (McNemar's test statistic (x^2) = 125.2, df =1, p-value<0.0001). Therefore the null hypothesis of equal performance of these two methods is rejected.

4.2.4. Application of the algorithm in Southern Africa

The MODIS fire product was used to validate the multi-temporal threshold algorithm (without CO_2 correction) developed in this study and compare the accuracy with that of the MSG FIRG product in Southern Africa.

4.2.4.1. Accuracy assessment of the MODIS fire product

The table 4.5 below shows the accuracy of MODIS fire product when ground fire data from Portugal was used for validation (Error matrix is shown in Appendix 11).

Table 4.5 Accuracy of the MODIS fire product

	Errors of commission (%)	Errors of omission (%)	Fires Detected (%)
MODIS Fire Product	29.8	35.9	64.1

4.2.4.2. Accuracy assessment of the algorithm in Southern Africa

The MODIS fire product has higher accuracy as compared to the multi-temporal threshold algorithm developed in this study as well as the MSG FIR-G product. This is mainly because of its high spatial resolution of 1km as compared to 3km for MSG satellite. Therefore the MODIS fire product was used as reference data to compare the accuracy of multi-temporal threshold algorithm with that of the MSG FIR-G product in Southern Africa. The map below (Figure 4.15) shows the comparison of the multi-temporal threshold algorithm and MSG FIR-G product in Southern Africa (parts of Angola, Botswana, Namibia, South Africa, Zambia and Zimbabwe) using the MODIS fire product for validation (see also Appendix 17).

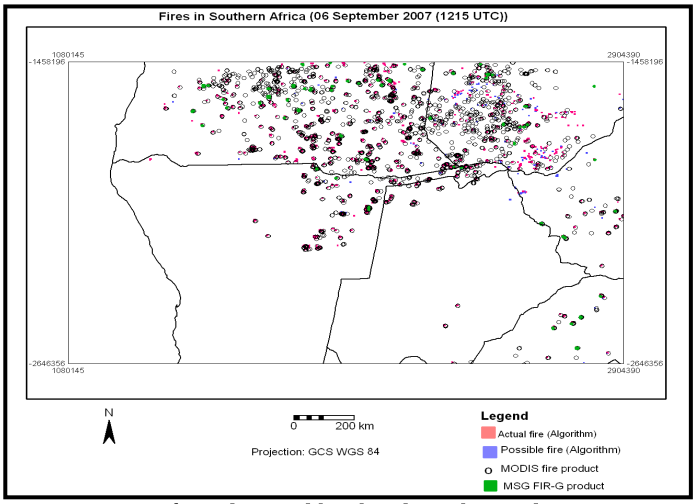

Figure 4.15 MODIS fires detected by the algorithm and MSG FIR-G product

The tables below show the statistics on accuracy and comparison of the multi-temporal threshold algorithm and MSG FIR-G product when MODIS fire product was used for validation in Southern Africa. These tables are based on the error matrices and frequency table in Appendix 12.

Table 4.6 Accuracy of the algorithms: (multi-temporal threshold algorithm and contextual threshold algorithm (MSG FIR-G product) when MODIS fire Product is used for validation)

	Errors of commission (%)	Errors of omission (%)	Fires Detected (%)
Multi-temporal threshold algorithm without	4.7	25.1	74.9
Contextual algorithm (MSG FIR-G)	1.6	87.9	12.1

Table 4.7 Frequency of correct and wrongly classified pixels by the multi-temporal threshold algorithm and contextual algorithm (MSG FIR-G product)

	Multi-temporal threshold algorithm without CO_2 correction		Total
MSG FIRG product (contextual algorithm)	Wrong	Correct	
Wrong	512	1296	1808
Correct	80	242	322
Total	592	1538	2130

The results show that the multi-temporal threshold algorithm has a higher accuracy compared to the contextual algorithm; this difference is significant (McNemar's test statistic (x^2) = 1074.6, df = 1, p-value<0.0001) and one can reject the null hypothesis of equal performance of the two algorithms.

4.3. The automated procedure for the multi-temporal threshold algorithm

The automation of the procedure outlined in figure 3.10 resulted in a semi-automated system that has three main scripts:

i) Create_solarzenithangle_maps - for calculating the solar zenith angles (Appendix 13)

ii) (a) Active_fire_detection_algorithm_v1.1 - for fire detection without using the cloud mask (Appendix 14)

(b) Active_fire_detection_algorithm_v1.2 - for fire detection including the use of cloud mask (Appendix 15)

iii) CLM_processing – for cloud mask processing (Appendix 16) and used when script in (ii) (b) above is used.

These scripts perform the batch processing of the procedures in figure 16. It takes less than 15 minutes to do the processing of all the procedures and come up with fire map. It was confirmed in this study that the results obtained through the use of these scripts are similar to the ones obtained by manually following all the procedures in the scripts.

The following steps have to be followed to fully execute the procedure for the multi-temporal threshold algorithm developed in this study:

1. Data retrieving - settings

The settings shown in figure 4.16 below should be set on the MSG data retriever when downloading the data for this algorithm. These specifications are important as they make it possible to repeat this research or whenever this algorithm is used.

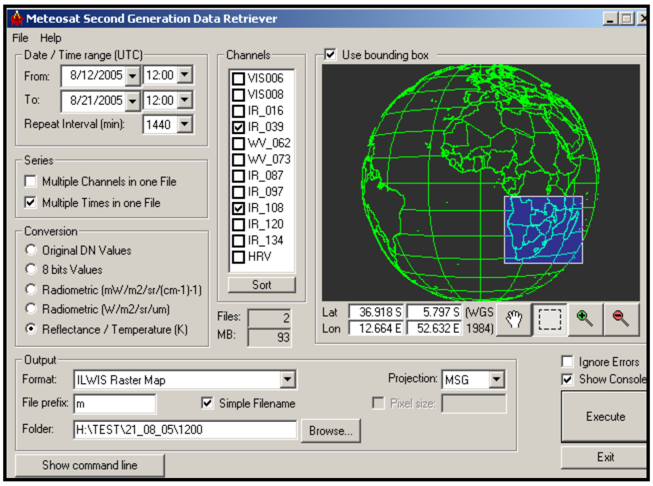

Figure 4.16 Settings on MSG data retriever

All the settings shown above are important as they are also specified in the scripts so if this is not done properly there could be some problems with the execution of the algorithm using these scripts. The file prefix should be specified as this is a parameter (%6) required in setting the georeference for the output solar zenith angle maps in step 2 below. This prefix is also required as a parameter (%9) in step 3 for the map lists file names. The default for this system is *"m"* but it can be changed to any other letter. If this is not specified it could be difficult to run the system. The images should be saved in the same directory with the scripts.

2. Generate solar zenith angles

Since the thresholds for fire detection are different for day, twilight and night conditions, it is necessary to calculate the solar zenith angles for the area of interest as these are inputs in the next step. This is done by running the create_solarzenithangle_maps script. When running this script some parameters have to be specified and these include: year, month, day, time, output georeference and the file prefix for the resampled solar zenith angles georeference. The file prefix is the same as specified in step 1 above. Time should be entered in this format: 12.00 (for 12:00 UTC).

3. Fire detection

When all is set, fire detection could be done by running the fire detection scripts. There are two versions of the fire detection algorithms:

(a) Active_fire_detection_algorithm_v1.1

(b) Active_fire_detection_algorithm_v1.2

These have same parameters that have to be specified and these include the thresholds for the algorithms (*f* values in 4.1.2) and the map list file name prefix specified in step 1. It should be noted that algorithm (a) should be used when there is no use of cloud mask and (b) requires the use of cloud mask. Therefore when using algorithm (b) the cloud mask should be processed using the CLM_processing script (Appendix 16). It is also worth to point out that these files should be in the same directory otherwise it could be difficult or impossible to run this automated procedure. Whenever algorithm (a) is used the visible channels should be used to check if the area of interest is free of clouds otherwise the results could be greatly affected by clouds. It should be noted that CO_2 correction was not considered at this stage since it does not improve the accuracy of the algorithm.

5. Discussion of results

This chapter discusses the results presented in Chapter 4 above, mainly focussing on the multi-temporal threshold algorithm, accuracy of the algorithm as well as the automation of the procedure for the algorithm.

5.1. Multi-temporal threshold algorithm

This study has proved that the temperature anomalies determined through the multi-temporal analysis can be used for forest fire detection. Only a few algorithms that consider the use of multi-temporal methods in forest fire detection have been developed so far and the results of this study have confirmed the conclusions made by other different multi-temporal algorithms (van den Bergh and Frost, 2005, Mazzeo et al., 2007, Koltunov and Ustin, 2007) that multi-temporal analysis can be used for forest fire detection. The thresholds for the multi-temporal algorithm for day and night are quite different due to the recording of the solar component during the day in IR3.9 channel; therefore the thresholds are higher during day time as compared to night time. The difference between IR3.9 and IR10.8 channels has been proved to be important in this study. This is important as the IR3.9 channel alone cannot be reliable for fire detection since this channel is very sensitive to temperature changes so it may be high even when there is no fire. Therefore the difference between IR3.9 and IR10.8 channels will give or increase the confidence on presence or absence of fire. The use of these two MSG channels has been applied in many algorithms for fire detection for example by Calle et al., (2004) and Hassini et al., (2009) and they also confirmed the difference between day and night thresholds. Although this algorithm is based on multi-temporal analysis, it has shown that it also requires the application of these two channels (IR3.9 and IR10.8) as in contextual algorithms mentioned above. The algorithm can be applied to any other geostationary satellites using the same channels (IR3.9 and IR10.8) for near real time forest fire detection. Only solar zenith angles in this algorithm are specific to MSG satellite as they are calculated from 0^0 latitude and 0^0 longitude so these need to be changed to suit the specifications of the particular geostationary satellite position.

5.2. Accuracy of the multi-temporal algorithm

The multi-temporal threshold algorithm developed in this study detected more fires as compared to the MSG FIR-G product that is based on contextual threshold concept. This is basically attributed to the differences in these methods as all other aspects such as time and spatial resolutions are similar. This was confirmed in both Portugal and Southern Africa. The use of these two study areas (Portugal (small or national scale) and Southern Africa (regional scale)) with different environments helped to clearly show the superiority of the multi-temporal algorithm developed in this study over the contextual algorithms. This also means that the algorithm can be applied to any location within the view of the MSG satellite. However the accuracy of the multi-temporal algorithm is not very high when the ground data is used for validation as compared to when the MODIS fire product is used. This may be due to several factors such as the errors in recording the time when the fire started and ended. Csizar et al., (2006) noted that the use of in situ observations of fire may be difficult to achieve as some of the fires may not have been recorded. This increases the false fire alarms (errors of commission). In this study this was mainly realized during the day as there could be some fires of short duration but with high intensity or high temperatures that could be picked up by the satellites. Giglio, (2007) confirmed by Hawbacker, (2008) noted that fire activity follows a diurnal or daily cycle often increasing in the afternoon when weather conditions are most favorable for burning. These fires are rarely recorded. In support of this, Calle et al., (2004) also noted that the validity of the fire detection rate of any algorithm lies in the quality of data used in the validation or accuracy assessment and errors of commission are most common in almost all forest fire detection models.

Although clouds were removed there are some clouds which are transparent and difficult to detect. Roberts and Wooster,(2008) noted that there is a tendency for some small clouds and edges of clouds that remain unmasked when the MSG CLM product is used. Flannigan and Von der Haar, (1986) in Hawbaker et al., (2008) pointed out that clouds are a most difficult factor that greatly disturbs the detection of forest fires by remote sensing. These clouds greatly lead to high errors of omission since they induce low temperatures so the fires under these clouds are not detected. These contaminated fires are included in the analysis and recorded as missed fires thereby increasing the errors of omission. This was also realized in this study especially during the twilight conditions (when solar zenith angle between 70 and 90^0). Hassini et al., (2009) also pointed out that there are some problems with these dusk and dawn periods as they experience a rapid change of temperatures especially in IR3.9 channel so some fires may be missed. However this method has shown one of the ways of minimising the problems or uncertainties caused by the mixed water and land scene surfaces as well as unknown land surface emissivity especially in channel IR3.9. These issues were highlighted by Hassini et al., (2009) as outstanding in their contextual algorithm as it requires a 3x3 matrix. The multi-temporal analysis method developed in this study is pixel based and there is no use of a 3x3 matrix as in contextual algorithms.

The fire detection rate of the multi-temporal threshold algorithm decreased with the decrease in fire sizes (ha). This is due to the low spatial resolution (3km) of MSG satellite. This is confirmed by the ability of the MODIS (1km spatial resolution) to pick up more fires of smaller sizes (>45ha) as compared to the MSG satellite. This study proved that the multi-temporal threshold algorithm can detect well the fires greater than 135 ha. However it should be noted that fire size (ha) is not the only factor that determines the possibility of fires being detected by the satellites. Some other factors such as fuel load, moisture levels and the weather conditions are also of great importance (Hawbaker et al., 2008) as they determine the intensity or temperature of fire thereby affecting the detection rate of the multi-temporal threshold algorithm developed in this study. It is worth to note that the multi-temporal threshold method also confirmed that the fires are more likely to be detected in IR3.9 and IR10.8 when the temperature deviates from the approximate normal background temperature (300^0 K) so those fires with low temperatures are hardly detected. It can be noted that when the size of the fire increases its temperature also increases thereby deviating from normal background temperature (Figure 2.5) (EUMETSAT and CGMS, 1999, Philip, 2007). This increases the probability of fires detected by the multi-temporal threshold method (Figure 4.9).

Although there are different multi-temporal methods developed before, results of their validation are difficult to compare with the results of this study. For example Mazzeo et al., (2007) developed their multi-temporal robust satellite technique (RST) for fire detection but they did not provide the detailed accuracy statistics of their algorithm. Koltunov and Ustin, (2007) confirmed that their non-linear Dynamic Detection Model (DDM) did not detect the occurrence of forest fires correctly but acknowledged that the multi-temporal method have the potential to detect fires if further improvements are made.

This study has also proved that CO_2 correction for absorption in IR3.9 channel does not improve the detection rate of the multi-temporal threshold algorithm. The thresholds for daytime did not change from the ones for the algorithm without CO_2 correction. This shows that the relationship between IR3.9 and IR10.8 is not altered during the day unlike during the night where IR10.8 is normally above IR3.9 (Figure 4.4) and after CO_2 correction IR3.9 temperature will be higher than IR10.8 temperatures hence the thresholds also change. It was shown that when CO_2 correction is conducted, even those areas without fires will have higher temperatures so this increases the errors of commission (false fire alarms). Depending on the thresholds some fires may even be missed as their temperature becomes lower than that of the non fire areas. Therefore CO_2 correction is not necessary when using the top of atmosphere (TOA) brightness temperatures to detect forest fires. This may explain why CO_2 correction is not considered in many contextual algorithms such as developed by Calle et al., (2004) and Hassini et al., (2009).

5.3. Automation of the procedure for multi-temporal algorithm

This study has shown one of the possible ways of automating the multi-temporal algorithm for near real time fire detection and monitoring using geostationary satellites. This automated procedure takes less than 15 minutes to run and provide the fire map which makes it possible for near-real time monitoring of forest fires as it can cope with the temporal resolution of MSG (15 minutes). This was only tested using two study areas (Portugal and Southern Africa) and since this study did not focus on the full disk of the MSG satellite, it was not tested on how much time it takes to process the full MSG disk images. However it should be noted that the time taken to run this algorithm depends on the size of the area of interest and the procedures that are executed by the scripts for example the one without cloud masking takes less time as compared to the one which requires cloud masking and gives better results. Most of the multi-temporal algorithms are not automated and in this study it was also not possible to compare with the contextual algorithms applied to the MSG FIR-G product. It is most likely that it is faster to automatically process the contextual algorithm as compared to multi-temporal algorithm. This is mainly because the contextual algorithms are based on one image while the multi-temporal algorithms are based on more than one image to derive the final result (fire map) which takes a longer time to compute. This study has shown the applicability of multi-temporal method in near real time detection of forest fires using the geostationary satellites considering their high temporal resolution that is appropriate for monitoring rapidly changing environmental phenomenon. This is also a robust fire detection method that can be applied over the whole year without problems with seasonal variations as the background temperature is calculated from images directly prior to the actual image on which the active forest fires are detected.

5.4. Limitations of the study

This study has three major limitations:

1. Lack of fire ground data for other areas (Southern Africa) for validation of the multi-temporal threshold algorithm. The MODIS fire product is not a perfect reference for validation of other fire products or algorithms since it also uses a contextual algorithm; however, it is the most accurate fire product currently available.
2. The multi-temporal threshold algorithm developed in this study was only tested during the fire season in both Portugal and Southern Africa so its performance throughout the year was not verified.
3. The validation was based on yes or no fire which was difficult to handle especially when MODIS fire product was used for validation due to the different spatial resolutions between MODIS (1km) and MSG (3km) satellites. Therefore one fire pixel or point in MSG may have more fire points in MODIS.

6. Conclusion & Recommendations

This chapter outlines the conclusions and recommendations of this study.

6.1. Conclusions

This study fulfilled the research objectives and answers the research questions outlined in section 1.3. The major conclusions of this study are outlined below:

MSG SEVIRI capability to detect temperature anomalies using the multi-temporal method

MSG satellite is capable of detecting the temperatures anomalies using the multi-temporal analysis method using the IR3.9 and IR10.8 channels. This is mainly due to the sensitivity of these channels to temperature changes which makes them capable of detecting the anomalies as the temperature for a particular time deviates from the normal background temperatures. These temperature anomalies can be used to detect forest fires.

The importance of the difference between IR3.9 and IR10.8 channels in forest fire detection using multi-temporal threshold algorithm

The difference between the IR3.9 and IR10.8 channels is important in forest fire detection using the multi-temporal method. This is mainly because the IR3.9 channel is very sensitive to temperature changes as compared to IR10.8 so the temperature in IR3.9 channel may be high as compared to the normal background temperatures even if there is no fire. Therefore the difference between these channels helps to discriminate fire pixels or points from non-fire pixels as the large difference signifies fire and small difference means low probability of fire.

How the temperature anomalies can be used to detect fires

Multi-temporal analysis method can be used to detect forest fires based on specified thresholds considering the temperature anomalies in IR3.9 and IR10.8 channels for MSG satellites. This method is applicable to day, night and twilight conditions and can be applied to the full MSG disk since it considers the different illumination conditions. These thresholds can be applied to other geostationary satellites. Only solar zenith angles in this algorithm are specific to MSG satellite as they are calculated from 0^0 latitude and 0^0 longitude so these can be changed to suit the specifications of a particular geostationary satellite.

The accuracy of the multi-temporal threshold algorithm

The multi-temporal threshold algorithm developed in this study has higher accuracy as compared to the contextual algorithm that is applied in MSG FIR-G product when either the ground fire data or MODIS fire product is used for validation. The difference in the performance of these algorithms is attributed to the fundamental differences in these methods as other factors such as spatial and temporal resolutions are similar. Undetected clouds were increasing the errors in fire detection using a multi-temporal threshold algorithm developed in this study.

IR3.9 CO_2 correction

CO_2 correction does not improve the accuracy of the multi-temporal threshold algorithm therefore it is not necessary in forest fire detection using the brightness temperature at the top of atmosphere (TOA).

Automation of the procedure for the multi-temporal threshold algorithm

The procedure was automated using scripts in ILWIS. The automated procedure for the multi-temporal threshold algorithm can cope with the temporal resolution of MSG satellite (15 minutes). Therefore it is applicable in near real time monitoring of forest fires which is a rapidly changing environmental phenomenon.

6.2. Recommendations

Based on the limitations and conclusions of this study the following recommendations are made:

- Further validation or accuracy assessment of the multi-temporal algorithm using ground data from different locations. The validation scheme may be improved especially when MODIS fire product is used for validation.
- Use of supplementary cloud mask in addition to MSG CLM (cloud mask) product to minimize the effects of clouds on the performance of the multi-temporal threshold algorithm.
- Apply the algorithm to other geostationary satellites to assess its performance.

The multi-temporal threshold algorithm developed in this study is robust and simple to apply in forest fire detection for near real time monitoring and it can be applied to other geostationary satellites such as GOES, MTSAT-1R and FY-2C and only the solar zenith angles have to be adjusted depending on the position of the satellite. Although the algorithm was only validated in Portugal and Southern Africa it is also applicable to other areas however this has to be confirmed through further studies.

Reference

Alleaume, S., Hély, C., Roux, J. L., Korontzi, S., Swap, R. J., Shugart, H. H. & Justice, C. O. (2005) Using MODIS to evaluate heterogeneity of biomass burning in southern African savannahs: a case study in Etosha. *International Journal of Remote Sensing,* 26**,** 4219-4237.

Arino, O. & Melinotte, J. M. (1998) The 1993 Africa fire map. *International Journal of Remote Sensing,* 19**,** 2019-2023.

Calle, A., Gonzalez-Alonso, F. & Merino de Miguel, S. (2008) Validation of active forest fires detected by MSG-SEVIRI by means of MODIS hot spots and AWiFS images. *International Journal of Remote Sensing,* 29**,** 3407-3415.

Calle, A., Romo, A., Sanz, J. & Casanova, J. L. (2004) Fire Detection and Monitoring, in Real Time, Using MSG Images. Proceedings of the Second MSG RAO Workshop (ESA SP-582). Salzburg, Austria, 9-10 September 2004. Organised by ESA, in cooperation with EUMETSAT. Editor: H. Lacoste, p. 65.

Campbell, J. B. (2006) *Introduction to Remote Sensing,* The Guilford Press.

Catry, F. X., Damasceno, P., Silva, J. S., Galante, M. & Moreira, F. (2007 (a)) Spatial Distribution Patterns of Wildfire Ignitions in Portugal. (Online), Available: http://www.eufirelab.org/toolbox2/library/upload/2380.pdf [acessed 2009, January 12]

Catry, F. X., Rego, F. C., Santos, T., Almeida, J. & Relvas, P. (2007 (b)) Forest Fires Prevention in Portugal-Using GIS to Help Improving Early Fire Detection Effectiveness. (Online), Available: http://www.isa.utl.pt/ceabn/uploads/docs/Forest_fires_prevention_paper.pdf [acessed 2009, January 10]

Christopher, S. A., Wang, M., Berendes, T. A., Welch, R. M. & Yang, S. K. (1998) The 1985 Biomass Burning Season in South America: Satellite Remote Sensing of Fires, Smoke, and Regional Radiative Energy Budgets. *Journal of Applied Meteorology,* 37**,** 661-678.

Csiszar, I. A., Morisette, J. T. & Giglio, L. (2006) Validation of active fire detection from moderate-resolution satellite sensors: the MODIS example in northern eurasia. *Geoscience and Remote Sensing, IEEE Transactions on,* 44**,** 1757-1764.

de Leeuw, J., Jia, H., Yang, L., Liu, X., Schmidt, K. & Skidmore, A. K. (2006) Comparing accuracy assessments to infer superiority of image classification methods. *International Journal of Remote Sensing,* 27**,** 223-232.

EUMETSAT (2007) Active Fire Monitoring with MSG Algorithm Theoretical Basis Document. (Online), Available: http://www.eumetsat.int/Home/Main/Publications/Technical_and_Scientific_Documentation/Technical_Notes/SP_1124282585834?l=en [acessed 2008, August 22].

EUMETSAT & CGMS (1999) Directory of Meteorological Satellites Applications. (Online), Available: http://www.wmo.ch/pages/prog/sat/CGMS/Directoryofapplications/en/ap2-11.htm [accessed 2008, August 25].

FIRMS (2008) Web fire mapper: Southern Africa. . (Online), Available: http://maps.geog.umd.edu/website/Activefire_HTML/viewer.htm?MAP=CSAFRICA-ArcIMSparam&DATALIST=,wc,wco,mafd24,mafd08,ER,RI,&BANNER=CSA_banner&ele_fire=fireAims&requiredMap=SouthernAfrica [accessed 2008, August 28].

Flannigan, M. D. & Vonder Haar, T. H. (1986) Forest fire monitoring using NOAA satellite AVHRR. *Canadian journal of forest research(Print),* 16**,** 975-982.

Flasse, S. P. & Ceccato, P. (1996) A contextual algorithm for AVHRR fire detection. *International Journal of Remote Sensing,* 17**,** 419-424.

Foody, G. M. (2001) Progress reports, GIS: the accuracy of spatial data revisited. *Progress in Physical Geography,* 25**,** 389-398.

Foody, G. M. (2004) Thematic map comparison: evaluating the statistical significance of differences in classification accuracy. *PE&RS, Photogrammetric Engineering & Remote Sensing,* 70**,** 627-633.

Frost, P. & Scholes, B. (2007) The Advanced Fire Information System. IN Secretariat, G. (Ed.) *The Future.* GEO 2007.

Gieske, A. S. M., Hendrikse, J., Retsios, V., Van Leeuwen, B., Maathuis, B. H. P., Romaguera, M., Sobrino, J. A., Timmermans, W. J. & Su, Z. (2005) Processing of msg-1 seviri data in the thermal infrared. Algorithm development with the use of the sparc2004 data set. *ESA/SPARC2004 Proceedings*.

Giglio, L. (2007) Characterization of the tropical diurnal fire cycle using VIRS and MODIS observations. *Remote Sensing of Environment,* 108**,** 407-421.

Giglio, L., Descloitres, J., Justice, C. O. & Kaufman, Y. J. (2003) An Enhanced Contextual Fire Detection Algorithm for MODIS. *Remote Sensing of Environment,* 87**,** 273-282.

Giglio, L., Kendall, J. D. & Justice, C. O. (1999) Evaluation of Global Fires Detection Algorithms Using Simulated AVHRR Infrared Data. *International Journal of Remote Sensing,* 20**,** 1947-1985.

Gomes, J. F. P. (2006) Forest fires in Portugal: how they happen and why they happen. *International Journal of Environmental Studies,* 63**,** 109-119.

Groot, W. J., Lynham, T. J., Brady, M. A., Csiszar, I. A., Davies, D., Justice, C. O., Prins, E. M. & Goldammer, J. G. (2007) Global Observation of forest and Land Cover Dynamics (GOFC-GOLD): monitoring and early warning systems for wildland fire disaster reduction. IN Secretariat, C. (Ed.) *The Future.* Geneva, GEO 2007.

Hassini, A., Benabdelouahed, F., Benabadji, N. & Belbachir, A. H. (2009) Active Fire Monitoring with Level 1.5 MSG Satellite Images. *American Journal of Applied Sciences,* 6**,** 157-166.

Hawbaker, T. J., Radeloff, V. C., Syphard, A. D., Zhu, Z. & Stewart, S. I. (2008) Detection rates of the MODIS active fire product in the United States. *Remote Sensing of Environment,* 112**,** 2656-2664.

IPCC (1995) *Climate Change 1995:The Science of Climate Change,* New York, Cambridge University Press.

Janssen, L. F. & Huurneman, G. C. (2001) *Principles of Remote Sensing,* Enschede, The Netherlands, ITC.

Justice, C. O., Giglio, L., korontzi, S., Owens, J., Morisette, J. T., Roy, D. P., Descloitres, J., Alleaume, S., Petitcolin, F. & Kaufman, Y. (2002) The MODIS fire products. *Remote Sensing of Environment,* 83**,** 244-262.

Kaufman, Y. J., Justice, C. O., Flynn, L. P., Kendall, J. D., Prins, E. M., Giglio, L., Ward, D. E., Menzel, W. P. & Setzer, A. W. (1998) Potential global fire monitoring from EOS-MODIS. *Journal of Geophysical Research,* 103**,** 32215-32238.

Kerkmann, J. (2004) Applications of Meteosat Second Genaration (MSG) : Meteorological Use of the SEVIRI IR3.9 Channel. EUMETSAT, (Online),Available: http://oiswww.eumetsat.org/WEBOPS/msg_interpretation/PowerPoints/Channels/Channel_IR39.ppt#370,1,Slide 1 [accessed 2008, October 28].

Koltunov, A. & Ustin, S. L. (2007) Early fire detection using non-linear multitemporal prediction of thermal imagery. *Remote Sensing of Environment,* 110**,** 18-28.

Li, Z., Nadon, S. & Cihlar, J. (2000) Satellite-based detection of Canadian boreal forest fires: development and application of the algorithm. *International Journal of Remote Sensing,* 21**,** 3057-3069.

Liew, S. C., Shen, C., Low, J., Lim, A. & Kwoh, L. K. (2003) Validation of MODIS fire product over Sumatra and Borneo using high resolution SPOT imagery. Proc. 24th Asian Conf. Remote Sensing and 2003 Int. Symp. Remote Sensing.

Longley, P., Goodchild, M. F., Maguire, D. J. & Rhind, D. W. (2005) *Geographic Information Systems and Science*, Wiley.

Mazzeo, G., Marchese, F., Filizzola, C., Pergola, N. & Tramutoli, V. (2007) A Multi-temporal Robust Satellite Technique (RST) for Forest Fire Detection. Analysis of Multi-temporal Remote Sensing Images, 2007. MultiTemp 2007. International Workshop.

Morisette, J. T., Giglio, L., Csiszar, I. & Justice, C. O. (2005) Validation of the MODIS active fire product over Southern Africa with ASTER data. *International Journal of Remote Sensing,* 26**,** 4239-4264.

Pereira, M. G., Trigo, R. M., Malamud, B. D., Pereira, J. M. C., DaCamara, C. C. & Calado, M. T. (2007) A Continental Portugal wildfire database. *Geophysical Research Abstracts,* 9**,** 09830.

Philip, S. (2007) Active Fire Detection Using Remote Sensing Based Polar-Orbiting and Geostationary Observations: An Approach Towards Near Real-Time Fire Monitoring. MSc Thesis, (Online), Available: http://www.gem-msc.org/Academic%20Output/Susan%20Philip.pdf [accessed 2008, August 28]

Powell, R. L., Matzke, N., de Souza, C., Clark, M., Numata, I., Hess, L. L. & Roberts, D. A. (2004) Sources of error in accuracy assessment of thematic land-cover maps in the Brazilian Amazon. *Remote Sensing of Environment,* 90**,** 221-234.

Prins, E., Govaerts, Y. & Csiszar, I. (2007) GOFC-GOLD Fire Monitoring and Mapping Implementation Team 2nd Workshop on Geostationary Fire Monitoring and Applications. Darmstadt, Germany, EUMETSAT.

Prins, E., McNamara, D. & Schmidt, C. (2004) Global Geostationary Fire Monitoring System. 13th Conference on Satellite Meteorology and Oceanography.

Roberts, G. J. & Wooster, M. J. (2008) Fire Detection and Fire Characterization Over Africa Using Meteosat SEVIRI. *IEEE Transactions On Geoscience And Remote Sensing,* 46.

ROCEA (2007) Fires in Africa: 1997 – 2005. (Online), Available: http://ochaonline.un.org/OchaLinkClick.aspx?link=ocha&docId=1087249 [accessed 2008, August 27]

Rosenfield, D. (2005) Application of Meteosat Second Gereneration (MSG): Conversion from Counts to Radiances and from Radiances to Brightness Temperature and Reflectances. EUMESAT, (Online),Available: http://oiswww.eumetsat.org/WEBOPS/msg_interpretation/PowerPoints/Channels/conversion_20050225.ppt#609,1,Slide 1 [accessed 2008, October 28].

Roy, D. P., Frost, P. G. H., Justice, C. O. & Landmann, T. (2005) The Southern Africa Fire Network (SAFNet) regional burned-area product-validation protocol. *International Journal of Remote Sensing,* 26**,** 4265-4292.

San-Miguel-Ayanz, J., Ravail, N., Kelha, V. & Ollero, A. (2005) Active fire detection for fire emergency management: Potential and limitations for the operational use of remote sensing. *Natural hazards(Dordrecht),* 35**,** 361-376.

Schmetz, J., Pili, P., Tjemkes, S., Just, D., Kerkmann, J., Rota, S. & Ratier, A. (2002) An Introduction to Meteosat Second Generation (MSG). *Bulletin of the American Meteorological Society,* 83**,** 977-992.

Shan-long, L. U., Xiao-hua, S. & Le-jun, Z. O. U. (2006) Land cover change in Ningbo and its surrounding area of Zhejiang Province, 1987~ 2000. *Journal of Zhejiang University - Science A,* 7**,** 633-640.

Stehman, S. V. (1999) Basic probability sampling designs for thematic map accuracy assessment. *International Journal of Remote Sensing,* 20**,** 2423-2441.

Strahler, A. H., Boschetti, L., Foody, G. M., Friedl, M. A., Hansen, M. C., Herold, M., Mayaux, P., Morisette, J., Stehman, S. & Woodcock, C. E. (2006) Global Land Cover Validation: Recommendations for Evaluation and Accuracy Assessment of Global Land Cover Maps. *European Communities, Luxembourg*.

Udahemuka, G., Van Wyk, B. J., Van Wyk, M. A. & Van den Bergh, F. (2008) Robust fitting of diurnal brightness temperature cycles: pattern recognition special edition. *South African Computer Journal,* 40**,** 31-36.

van den Bergh, F. & Frost, P. E. (2005) A multi temporal approach to fire detection using MSG data;Analysis of Multi-Temporal Remote Sensing Images, 2005 International Workshop Analysis of Multi-Temporal Remote Sensing Images, 2005 International Workshop

WoF (2008) Working on Fire Programme: a brief history. (Online), Available: http://www.workingonfire.org/history.php [accessed 2008, October 25]

Appendices

Appendix 1

Conversion from Radiances to brightness temperature (Gieske et al., 2005)
The formula below is used to convert the radiances to brightness temperatures for MSG satellite:

$$T_b = \left[C_2 \nu_c / \log\left(\frac{C_1 \nu_c^3}{R} + 1 \right) - B \right] / A$$

Where C_1 = 1.19104 10-5 mW m-2 sr-1(cm-1)-4
C_2 = 1.43877 K (cm-1)-1
ν_c = central wavenumber of the channel
A, B coefficients (see table below)

Values for the central wavenumber (in cm^{-1}), and the parameters A, and B (in K) for the thermal infrared MSG SEVIRI channels used in the equation.

Channel No	Channel ID	ν_c	A	B
04	IR3.9	2569.094	0.9959	3.471
05	WV6.2	1598.566	0.9963	2.219
06	WV7.3	1362.142	0.9991	0.485
07	IR8.7	1149.083	0.9996	0.181
08	IR9.7	1034.345	0.9999	0.060
09	IR10.8	930.659	0.9983	0.627
10	IR12.0	839.661	0.9988	0.397
11	IR13.4	752.381	0.9981	0.576

Appendix 2

Tests and training of the algorithm to determine the thresholds

Night (Solar zenith angle >90^0)

(i) Actual fire

$$dT_{3.9\mu m} > m_{t(3.9\mu m)} + f_1(S_{t(3.9\mu m)})$$

$$T_{dif} > m_{dif} + f_2\,(S_{dif})$$

(iv) Probable fire

$$dT_{3.9\mu m} > m_{t(3.9\mu m)} + f_3(S_{t(3.9\mu m)}) < m_{t(3.9\mu m)} + f_1(S_{t(3.9\mu m)})$$

$$T_{dif} > m_{dif} + f_4(S_{dif}) < m_{dif} + f_2(S_{dif})$$

Thresholds				**Producer's accuracy (%)**	**User's accuracy (%)**
f₁	***f₂***	***f₃***	***f₄***		
1.5	3	0	0	18.5	96.6
1	1	0	0	15.9	92.3
1.5	1.5	0	0	16.6	96.2
2	2	0	0	17.2	96.3
1.5	2	0	0	17.9	96.4
2	3	0	0	17.9	93.1
2.5	2.5	0	0	17.2	92.8
2.5	3	0	0	17.9	96.4
1	**3**	**0**	**0**	**19.2**	**100**
1.5	1.5	1	1	17.9	96.4
2	2	1	1	17.2	96.2
2.5	2.5	1	1	16.6	96.1
3	3	1	1	16.6	100

Appendix 3

Tests and training of the algorithm to determine the thresholds

(i) Actual fire

$$dT_{3.9\mu m} > m_{t(3.9\mu m)} + f_1(S_{t(3.9\mu m)})$$
$$T_{dif} > m_{dif} + f_2\,(S_{dif})$$

(ii) Probable fire

$$dT_{3.9\mu m} > m_{t(3.9\mu m)} + f_3(S_{t(3.9\mu m)}) < m_{t(3.9\mu m)} + f_1(S_{t(3.9\mu m)})$$
$$T_{dif} > m_{dif} + f_4(S_{dif}) < m_{dif} + f_2(S_{dif})$$

Day (Solar zenith angle <70^0)

Thresholds				Producer's accuracy (%)	User's accuracy (%)
f₁	***f₂***	***f₃***	***f₄***		
1.5	1.5	1	1	22.1	69.8
2	2	1	1	19.9	61.4
3	3	1	1	20.5	63.6
2.5	**3**	**2**	**2.5**	**22.1**	**85.7**
3	3	1.5	1.5	19.1	74.3
2.5	2.5	2	2	22.1	71.4
4	4	2	2	17.6	85.7
2.5	2.5	1.5	1.5	22.1	71.4
4	5	2	2.5	14.0	90.4
4	5	3	3	11.0	93.8
5	5	3.5	3.5	11.8	84.2
4	5	2.5	3	11.8	84.2

Appendix 4

Tests and training of the algorithm to determine the thresholds

Twilight conditions (Solar zenith angle >70 and <90)

Linear interpolation

(i) Actual fire

$$dT_{3.9\mu m} > m_{t(3.9\mu m)} + f_1(S_{t(3.9\mu m)})$$

$$T_{dif} > m_{dif} + f_2(S_{dif})$$

(ii) Probable fire

$$dT_{3.9\mu m} > m_{t(3.9\mu m)} + f_3(S_{t(3.9\mu m)}) < m_{t(3.9\mu m)} + f_1(S_{t(3.9\mu m)})$$

$$T_{dif} > m_{dif} + f_4(S_{dif}) < m_{dif} + f_2(S_{dif})$$

$$y = y_a + \frac{(x - x_a)(y_b - y_a)}{(x_b - x_a)}$$

For f_1 $x_a = 90$ $x_b = 70$ $y_a = 0$ $y_b = 2$	For f_2 $x_a = 90$ $x_b = 70$ $y_a = 0$ $y_b = 2.5$
For f_3 $x_a = 90$ $x_b = 70$ $y_a = 1$ $y_b = 2.5$	For f_4 $x_a = 90$ $x_b = 70$ $y_a = 3$ $y_b = 3$

Appendix 5

Sensitivity analysis for determining the size of fires that can be detected by the algorithm.

Size of fires	Producer's accuracy (%)	User's accuracy (%)	Overall Accuracy (%)
> 22.5	37.1	83.7	34.6
>45.0	37.8	83.1	35.1
>67.5	39.9	79.4	36.2
>90.0	43.6	78.3	38.9
>112.5	44.2	76.3	39.2
>135.0	**45.8**	**76.3**	**40.1**
>157.5	44.8	74.7	38.9
>180	44.4	74.1	38.4

Appendix 6

Tests and training of the algorithm to determine the thresholds (with CO_2 correction)

Night (Solar zenith angle >90^0)

(i) Actual fire

$$dT_{3.9\mu m} > m_{t(3.9\mu m)} + f_1(S_{t(3.9\mu m)})$$

$$T_{dif} > m_{dif} + f_2(S_{dif})$$

(v) Probable fire

$$dT_{3.9\mu m} > m_{t(3.9\mu m)} + f_3(S_{t(3.9\mu m)}) < m_{t(3.9\mu m)} + f_1(S_{t(3.9\mu m)})$$

$$T_{dif} > m_{dif} + f_4(S_{dif}) < m_{dif} + f_2(S_{dif})$$

Thresholds				Producer's accuracy (%)	User's accuracy (%)
f_1	f_2	f_3	f_4		
5.5	6.0	4.5	4.5	28.4	44.7
6.0	6.5	5.0	5.0	27.0	46.5
6.0	7.5	5.5	5.5	27.0	47.6
7.0	7.5	6.0	6.5	25.6	52.8

Appendix 7

Tests and training of the algorithm to determine the thresholds (with CO_2 correction)

Day (Solar zenith angle <70^0)

(i) Actual fire

$$dT_{3.9\mu m} > m_{t(3.9\mu m)} + f_1(S_{t(3.9\mu m)})$$

$$T_{dif} > m_{dif} + f_2 (S_{dif})$$

(vi) Probable fire

$$dT_{3.9\mu m} > m_{t(3.9\mu m)} + f_3(S_{t(3.9\mu m)}) < m_{t(3.9\mu m)} + f_1(S_{t(3.9\mu m)})$$

$$T_{dif} > m_{dif} + f_4(S_{dif}) < m_{dif} + f_2(S_{dif})$$

Thresholds				**Producer's accuracy (%)**	**User's accuracy (%)**
f_1	***f_2***	***f_3***	***f_4***		
2.5	**3**	**2.0**	**2.5**	**50.0**	**60.7**
3.0	3.5	2.5	3.0	47.3	68.6
3.5	4.0	3.0	3.5	41.9	68.9
4.0	4.5	3.5	4.0	40.5	85.7

Appendix 8

Times for validation (Using ground data from Portugal)

CO_2 correction and no correction CO_2 correction

Date	Time UTC
06/09/07 and 07/09/07	0130-0300 1200-1300 1730-1830 1930-2030

Multi-temporal algorithm and MSG FIRG product

Date	Time UTC
06/09/07	0130-0230 1730-1830 1930-2030
07/09/07	0130-0230 0630-0730 1200-1300

Appendix 9

Accuracy assessment of the algorithms using ground data from Portugal

(a) Error Matrix for multi-temporal threshold algorithm, when it was individually assessed

	Ground data			
	Fire	Yes	No	Total
Fire map	Yes	27	7	34
	No	27		
	Total	54		

(b) Error Matrix for contextual algorithm (MSG FIRG product), when it was individually assessed

	Ground data			
	Fire	Yes	No	Total
Fire map	Yes	2	0	2
	No	52		
	Total	54		

(c) Frequency of two alternative methods (multi-temporal threshold algorithm and contextual threshold algorithm (MSG FIRG product)) compared against single reference data set from Portugal

Ground truth	Multi-temporal threshold algorithm	MSG FIRG product (Contextual algorithm)	Frequency
Fire	Fire	Fire	5
Fire	Fire	No fire	22
No fire	No fire	Fire	0
Fire	No fire	Fire	2
No fire	Fire	No fire	7
Fire	No fire	No fire	25
No fire	Fire	Fire	0

Appendix 10

Accuracy assessment of the multi-temporal algorithms (with and without CO_2 correction) using ground data from Portugal

(a) Error Matrix for Multi-temporal threshold algorithm without CO_2 correction, when it was individually assessed

	Ground data			
Fire map	Fire	Yes	No	Total
	Yes	32	20	52
	No	30	[redacted]	
	Total	62		

(b) Error Matrix for Multi-temporal threshold algorithm with CO_2 correction, when it was individually assessed

	Ground data			
Fire map	Fire	Yes	No	Total
	Yes	30	179	209
	No	32	[redacted]	
	Total	62		

(c) Frequency of two alternative methods (multi-temporal threshold algorithms (without CO_2 correction and one with CO_2 correction) compared against single reference data set (Ground data from Portugal)

Ground truth	Multi-temporal threshold algorithm without CO_2 correction	Multi-temporal threshold algorithm with CO_2 correction	Frequency
Fire	Fire	Fire	27
Fire	Fire	No fire	5
No fire	No fire	Fire	179
Fire	No fire	Fire	3
No fire	Fire	No fire	20
Fire	No fire	No fire	27
No fire	Fire	Fire	0

Appendix 11

Accuracy assessment of MODIS fire product

Error Matrix for MODIS fire product with reference to ground data from Portugal

	Ground data			
	Fire	Yes	No	Total
MODIS Fire product	Yes	134	57	191
	No	75	[redacted]	
	Total	209		

Appendix 12

Accuracy assessment of the algorithms using MODIS fire product

(a) Error Matrix for Multi-temporal threshold algorithm without CO_2 correction, it was individually assessed

	MODIS fire product			
	Fire	Yes	No	Total
Multi-temporal threshold algorithm without CO_2 correction Fire map	Yes	1536	76	1612
	No	516	[redacted]	
	Total	2052		

(b) Error Matrix for contextual algorithm (MSG FIRG product), when it was individually assessed

	MODIS fire product			
	Fire	Yes	No	Total
MSG FIRG product	Yes	248	4	252
	No	1804	[redacted]	
	Total	2052		

(c) Frequency of two alternative methods (multi-temporal threshold algorithm and contextual threshold algorithm (MSG FIRG product) compared against single reference data set (MODIS fire product)

MODIS	Multi-temporal threshold algorithm without CO2 correction	MSG FIRG Product	Frequency
Fire	Fire	Fire	242
Fire	Fire	No fire	1294
No fire	No fire	Fire	2
Fire	No fire	Fire	6
No fire	Fire	No fire	74
Fire	No fire	No fire	510
No fire	Fire	Fire	2

Appendix 13

Create_solarzenithangles_maps (ILWIS script)

Rem: Calculate satellite, sun zenith angle and sun elevation / illumination condition, for MSG projection
Rem: The output georeference should be avaialble, first import using the data retriever the required MSG images
Rem: Made by: Tawanda Manyangadze
Rem: Date: 10-02-09
Rem: Version: 1.1 for actvive fire detection algorithm version 1.1

Rem: Call external batch file, called generate angles.bat
!generateangles.bat %1 %2 %3 %4

copy sunzen*.* solzen

solzen:=map('solzen',genras,Convert,378,0,Real,4,SwapBytes)

setgrf solzen.mpr %5

Rem: Resampl solar zenith angles

solzen_r=MapResample(solzen.mpr,%60000.grf,BiCubic)

Rem: Give the undefined pixels (above 90) a value of 90.1 so that they can be assigned a threshold value
solzen_re:=ifundef(solzen_r,90.1,solzen_r)
//show solzen_re.mpr
closeall

Input parameters
%1 – Year
%2 – Month
%3 – Day
%4 – Time (UTC)
%5 – Output georeference
%6 - Input map list georef name prefix (for resampling angle map)

generateangles.bat - is a Java Applet developed at ITC to calculate angles for sun and MSG satellite.

Appendix 14

Active_fire_detection_algorithm_v1.1 (ILWIS script)

```
REM: Multi-temporal algorithm for active fire detection for near-real time
     monitoring using geostationary algorithm
REM: Made by: Tawanda Manyangadze
REM: Version: 1:1 (no use of cloud mask)
REM: Date: 10-02-09

//Creating a map list of the images of day -1 to -9 in IR3.9 channel
crmaplist b0_39 %90000_band_1.mpr %90000_band_2.mpr %90000_band_3.mpr
     %90000_band_4.mpr %90000_band_5.mpr %90000_band_6.mpr
     %90000_band_7.mpr %90000_band_8.mpr %90000_band_9.mpr

//Average temperature the past 9 days
Avg_039_9=MapMaplistStatistics(b0_39.mpl, Avg, 0, 8)

//Remove anomalies in the past 9 days
b1_039.mpl = maplistcalculate("iff(@1>(Avg_039_9-3),@1,0)",0,8,b0_39.mpl)
calc b1_039.mpl

b2_039.mpl = maplistcalculate("iff(@1<(Avg_039_9+3),@1,0)",0,8,b1_039.mpl)
calc b2_039.mpl

//Count- Removing all the days with anomalies in the past 9 days-assigned 0 in the
     previous operation
b2_039_count = maplistcalculate("iff(@1>0,@1,?)",0,8,b2_039.mpl)
calc b2_039_count.mpl

count_b2_039 = MapMaplistStatistics(b2_039_count.mpl, Cnt, 0, 8)

//Average temperature without the anomalies for the past 9 days
sum_b2_039 = MapMaplistStatistics(b2_039.mpl, Sum, 0, 8)

Avg_b2_039 = sum_b2_039/count_b2_039

// Difference between IR3.9 and IR 10.8

  //Creating a map list of the images of day -1 to -9 in IR10.8 channel
crmaplist b_108 %90001_band_1.mpr %90001_band_2.mpr %90001_band_3.mpr
     %90001_band_4.mpr %90001_band_5.mpr %90001_band_6.mpr
     %90001_band_7.mpr %90001_band_8.mpr %90001_band_9.mpr
calc b_108.mpl

  //Remove anomalies in the past 9 days
b2_108.mpl = maplistcalculate("iff(@1>0,@2,0)",0,8,b2_039.mpl,b_108.mpl)
calc b2_108.mpl
```

```
b2_count_108 = maplistcalculate("iff(@1>0,@1,?)",0,8,b2_108.mpl)
calc b2_count_108.mpl

    //IR3.9-IR10.8
diff_1 = maplistcalculate("@1-@2",0,8,b2_039.mpl,b2_108.mpl)
calc diff_1.mpl

    //Average difference between IR3.9 and IR10.8 (without anomalies) for
        previous 9 days
sum_diff = MapMaplistStatistics(diff_1.mpl, Sum, 0, 8)

Avg_diff = sum_diff/count_b2_039


//Standard deviation of IR3.9 channel

    //IR3.9 - average (x-m)
std_039_1.mpl = maplistcalculate("@1-Avg_b2_039",0,8,b2_039_count.mpl)
calc std_039_1.mpl

    //IR3.9 - average squared (x-m)2
std_039_2.mpl = maplistcalculate("@1^2",0,8,std_039_1.mpl)
calc std_039_2.mpl

    //Remove the anomalies
std_039_3.mpl                                                    =
        maplistcalculate("iff(@1>0,@2,@1)",0,8,b2_039.mpl,std_039_2.mpl)
calc std_039_3.mpl

   //Sum (x-m)2
sum_std_039 = MapMaplistStatistics(std_039_3.mpl, Sum, 0, 8)

  //Standard deviation IR3.9
std_039 = SQRT(sum_std_039/count_b2_039 )

//Standard deviation for IR3.9-IR10.8

   //Difference without anomalies
diff_2.mpl = maplistcalculate("@1-@2",0,8,b2_039_count.mpl,b2_count_108.mpl)
calc diff_2.mpl

  //Difference - average diff (x-m)
std_dif_1.mpl = maplistcalculate("@1-Avg_diff",0,8,diff_2.mpl)
calc std_dif_1.mpl
```

```
      //Difference - average diff squared (x-m)2
std_dif_2.mpl = maplistcalculate("@1^2",0,8,std_dif_1.mpl)
calc std_dif_2.mpl

      //Remove the anomalies
std_dif_3.mpl = maplistcalculate("iff(@1=0,@1,@2)",0,8,diff_1.mpl,std_dif_2.mpl)
calc std_dif_3.mpl

    //Sum (x-m)2
sum_std_dif = MapMaplistStatistics(std_dif_3.mpl, Sum, 0, 8)

  //Standard deviation IR3.9
std_dif= SQRT(sum_std_dif/count_b2_039)


//Thresholds
     //  Temperature for the 10th day which is day 1 in this analysis. If temperature in
            IR3.9 channel is less than in IR10.8 there is no possibility of fire
tmp_039_10=iff(%90000_band_10>%90001_band_10,%90000_band_10,?)

     //Difference IR3.9 - IR10.8 for day 1
dif_1_10=%90000_band_10-%90001_band_10

   //Remove clouds on the difference and negative difference mean no fire so should
            be removed
dif_2_10=iff(dif_1_10>0,dif_1_10,?)

    //To calculate f1
solzen_1= iff(solzen_re<70,%2,solzen_re)
solzen_2=   iff((solzen_1>70)and(solzen_1<90),%1+(((solzen_1-90)*(%2-%1))/(70-
            90)),solzen_1)
solzen_3= iff(solzen_2>90,%1,solzen_2)
//show solzen_3

//To calculate f2
solzen_4= iff(solzen_re<70,%4,solzen_re)
solzen_5=   iff((solzen_4>70)and(solzen_4<90),%3+(((solzen_4-90)*(%4-%3))/(70-
            90)),solzen_4)
solzen_6= iff(solzen_5>90,%3,solzen_5)
//show solzen_6

//To calculate f3
solzen_7= iff(solzen_re<70,%6,solzen_re)
solzen_8=   iff((solzen_7>70)and(solzen_7<90),%5+(((solzen_7-90)*(%6-%5))/(70-
            90)),solzen_7)
solzen_9= iff(solzen_8>90,%5,solzen_8)
```

```
//show solzen_9

//To calculate f4
solzen_10= iff(solzen_re<70,%8,solzen_re)
solzen_11=    iff((solzen_10>70)and(solzen_10<90),%7+(((solzen_10-90)*(%8-
     %7))/(70-90)),solzen_10)
solzen_12= iff(solzen_11>90,%7,solzen_11)
//show solzen_12

  //Fires  in IR3.9 channel
fires_039=iff(tmp_039_10>Avg_b2_039+solzen_3*std_039,tmp_039_10,?)

  //Fires (using the difference between IR3.9 and IR10.8)
fires_dif=iff(dif_2_10>(Avg_diff+solzen_6*std_dif),dif_2_10,?)

  //Fires combined IR3.9 and the difference between IR3.9 and IR10.8
fires_1=iff((fires_039>Avg_b2_039+solzen_9*std_039)and(fires_dif>Avg_diff+sol
     zen_12*std_dif),1,0)

fires_2=iff((fires_039<Avg_b2_039+solzen_9*std_039)and(fires_dif<Avg_diff+sol
     zen_12*std_dif),1,0)

fires_all=iff(fires_1=1,2,iff(fires_2=1,1,?))

  // The average and standard deviation of the past 3 days may give the
     approximate background temperature without the anomalies
fires_final=iff(count_b2_039>2,fires_all,?)
show fires_final.mpr
```

Input Parameters

%1 – First threshold night (f_3)
%2 – First threshold day (f_3)
%3 – Second threshold night (f_4)
%4 – Second threshold day (f_4)
%5 – Third threshold night (f_2)
%6 – Third threshold day (f_2)
%7 – Fourth threshold night (f_1)
%8 – Fourth threshold day (f_1)
%9 – Input map list name prefix (default ‘m’)

These are set as defaults in the script and for *f* values refer to results section 4.1.2

Appendix 15

Active_fire_detection_algorithm_v1.2 (ILWIS script)

```
REM: Multi-temporal algorithm for active fire detection for near-real time
     monitoring using geostationary algorithm
REM: Made by: Tawanda Manyangadze
REM: Version: 1:2 (with use of cloud mask)
REM: Date: 10-02-09

//Creating a map list of the images of day -1 to -9 in IR3.9 channel
crmaplist b0_39 %90000_band_1.mpr %90000_band_2.mpr %90000_band_3.mpr
     %90000_band_4.mpr %90000_band_5.mpr %90000_band_6.mpr
     %90000_band_7.mpr %90000_band_8.mpr %

90000_band_9.mpr

//Average temperature the past 9 days
Avg_039_9=MapMaplistStatistics(b0_39.mpl, Avg, 0, 8)

//Remove anomalies in the past 9 days
b1_039.mpl = maplistcalculate("iff(@1>(Avg_039_9-3),@1,0)",0,8,b0_39.mpl)
calc b1_039.mpl

b2_039.mpl = maplistcalculate("iff(@1<(Avg_039_9+3),@1,0)",0,8,b1_039.mpl)
calc b2_039.mpl

//Count- Removing all the days with anomalies in the past 9 days-assigned 0 in the
     previous operation
b2_039_count = maplistcalculate("iff(@1>0,@1,?)",0,8,b2_039.mpl)
calc b2_039_count.mpl

count_b2_039 = MapMaplistStatistics(b2_039_count.mpl, Cnt, 0, 8)

//Average temperature without the anomalies for the past 9 days
sum_b2_039 = MapMaplistStatistics(b2_039.mpl, Sum, 0, 8)

Avg_b2_039 = sum_b2_039/count_b2_039

// Difference between IR3.9 and IR 10.8

  //Creating a map list of the images of day -1 to -9 in IR10.8 channel
crmaplist b_108 %90001_band_1.mpr %90001_band_2.mpr %90001_band_3.mpr
     %90001_band_4.mpr %90001_band_5.mpr %90001_band_6.mpr
     %90001_band_7.mpr %90001_band_8.mpr %90001_band_9.mpr
calc b_108.mpl
```

```
   //Remove anomalies in the past 9 days
b2_108.mpl = maplistcalculate("iff(@1>0,@2,0)",0,8,b2_039.mpl,b_108.mpl)
calc b2_108.mpl

b2_count_108 = maplistcalculate("iff(@1>0,@1,?)",0,8,b2_108.mpl)
calc b2_count_108.mpl

    //IR3.9-IR10.8
diff_1 = maplistcalculate("@1-@2",0,8,b2_039.mpl,b2_108.mpl)
calc diff_1.mpl

     //Average difference between IR3.9 and IR10.8 (without anomalies) for
         previous 9 days
sum_diff = MapMaplistStatistics(diff_1.mpl, Sum, 0, 8)

Avg_diff = sum_diff/count_b2_039

//Standard deviation of IR3.9 channel

    //IR3.9 - average (x-m)
std_039_1.mpl = maplistcalculate("@1-Avg_b2_039",0,8,b2_039_count.mpl)
calc std_039_1.mpl

    //IR3.9 - average squared (x-m)2
std_039_2.mpl = maplistcalculate("@1^2",0,8,std_039_1.mpl)
calc std_039_2.mpl

    //Remove the anomalies
std_039_3.mpl=
         maplistcalculate("iff(@1>0,@2,@1)",0,8,b2_039.mpl,std_039_2.mpl)
calc std_039_3.mpl

   //Sum (x-m)2
sum_std_039 = MapMaplistStatistics(std_039_3.mpl, Sum, 0, 8)

  //Standard deviation IR3.9
std_039 = SQRT(sum_std_039/count_b2_039 )

//Standard deviation for IR3.9-IR10.8

   //Difference without anomalies
diff_2.mpl = maplistcalculate("@1-@2",0,8,b2_039_count.mpl,b2_count_108.mpl)
calc diff_2.mpl

  //Difference - average diff (x-m)
std_dif_1.mpl = maplistcalculate("@1-Avg_diff",0,8,diff_2.mpl)
```

```
calc std_dif_1.mpl

      //Difference - average diff squared (x-m)2
std_dif_2.mpl = maplistcalculate("@1^2",0,8,std_dif_1.mpl)
calc std_dif_2.mpl

      //Remove the anomalies
std_dif_3.mpl = maplistcalculate("iff(@1=0,@1,@2)",0,8,diff_1.mpl,std_dif_2.mpl)
calc std_dif_3.mpl

    //Sum (x-m)2
sum_std_dif = MapMaplistStatistics(std_dif_3.mpl, Sum, 0, 8)

  //Standard deviation IR3.9
std_dif= SQRT(sum_std_dif/count_b2_039)

//Thresholds

     //  Temperature for the 10th day which is day 1 in this analysis. If temperature in
          IR3.9 channel is less than in IR10.8 there is no possibility of fire
tmp_039_1=iff(%90000_band_10>%90001_band_10,%90000_band_10,?)

  //Remove Clouds on the 10th day
tmp_39_10=tmp_039_1*CLM

tmp_039_10=iff(tmp_39_10>0,tmp_39_10,?)

     //Difference IR3.9 - IR10.8 for day 1
dif_1_10=%90000_band_10-%90001_band_10

      //Remove clouds on the difference
dif_2_1=dif_1_10*CLM

// Negative difference mean no fire so should be removed
dif_2_10=iff(dif_2_1>0,dif_2_1,?)

    //To calculate f1
solzen_1= iff(solzen_re<70,%2,solzen_re)
solzen_2=   iff((solzen_1>70)and(solzen_1<90),%1+(((solzen_1-90)*(%2-%1))/(70-
          90)),solzen_1)
solzen_3= iff(solzen_2>90,%1,solzen_2)
//show solzen_3

//To calculate f2
solzen_4= iff(solzen_re<70,%4,solzen_re)
```

```
solzen_5= iff((solzen_4>70)and(solzen_4<90),%3+(((solzen_4-90)*(%4-%3))/(70-90)),solzen_4)
solzen_6= iff(solzen_5>90,%3,solzen_5)
//show solzen_6

//To calculate f3
solzen_7= iff(solzen_re<70,%6,solzen_re)
solzen_8= iff((solzen_7>70)and(solzen_7<90),%5+(((solzen_7-90)*(%6-%5))/(70-90)),solzen_7)
solzen_9= iff(solzen_8>90,%5,solzen_8)
//show solzen_9

//To calculate f4
solzen_10= iff(solzen_re<70,%8,solzen_re)
solzen_11= iff((solzen_10>70)and(solzen_10<90),%7+(((solzen_10-90)*(%8-%7))/(70-90)),solzen_10)
solzen_12= iff(solzen_11>90,%7,solzen_11)
//show solzen_12

  //Fires  in IR3.9 channel
fires_039=iff(tmp_039_10>Avg_b2_039+solzen_3*std_039,tmp_039_10,?)

   //Fires (using the difference between IR3.9 and IR10.8)
fires_dif=iff(dif_2_10>(Avg_diff+solzen_6*std_dif),dif_2_10,?)

  //Fires combined IR3.9 and the difference between IR3.9 and IR10.8
fires_1=iff((fires_039>Avg_b2_039+solzen_9*std_039)and(fires_dif>Avg_diff+solzen_12*std_dif),1,0)

fires_2=iff((fires_039<Avg_b2_039+solzen_9*std_039)and(fires_dif<Avg_diff+solzen_12*std_dif),1,0)

fires_all=iff(fires_1=1,2,iff(fires_2=1,1,?))

   // The average and standard deviation of the past 3 days may give the approximate background temperature without the anomalies
fires_final=iff(count_b2_039>2,fires_all,?)
show fires_final.mpr
```

Input parameters

%1 – First threshold night (f_3)
%2 – First threshold day (f_3)
%3 – Second threshold night (f_4)
%4 – Second threshold day (f_4)
%5 – Third threshold night (f_2)
%6 – Third threshold day (f_2)

%7 – Fourth threshold night (f_1)
%8 – Fourth threshold day (f_1)
%9 – Input map list name prefix (default ‘m’)

These are set as defaults in the script and for *f* values refer to results section 4.1.2

Appendix 16

CLM_processing (ILWIS script)

REM: Cloud mask processing

CLM_1=MapResample(%1,%20000.grf,BiCubic)

CLM=iff(CLM_1=1,1,0)

closeall

Input Parameters
%1 – Cloud mask file name
%2 – Georeference prefix name

Appendix 17

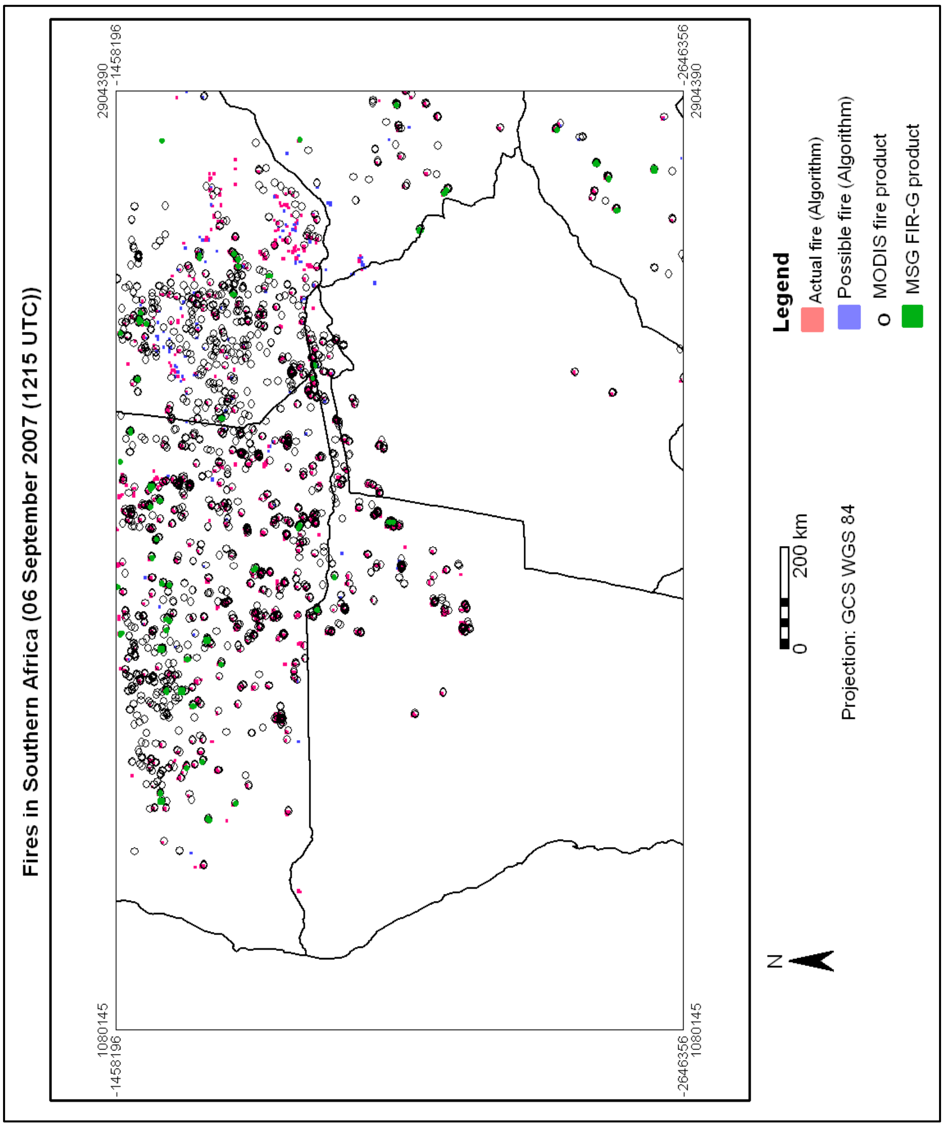

Fires in Southern Africa (06 September 2007 (1215 UTC))
2904390
-1458196
-2646356
2904390
1080145
-1458196
-2646356
1080145
Legend
Actual fire (Algorithm)
Possible fire (Algorithm)
MODIS fire product
MSG FIR-G product
0
200 km
Projection: GCS WGS 84
N